INCOHIS 2025 AUTUMN

NOV 8 -9, 2025
UNIVERSITY OF TRAVNIK/ BOSNIA AND HERZEGOVINA

INTERNATIONAL CONGRESS OF NEW HORIZONS IN SCIENCE AND SOCIAL SCIENCES

SCIENCES PROCEEDINGS BOOK



WWW.INCOHIS.COM

INCOHIS 2025 AUTUMN

INTERNATIONAL CONGRESS OF NEW HORIZONS IN

SCIENCE AND SOCIAL SCIENCES

SCIENCES PROCEEDINGS BOOK

NOV 8 – 9, 2025

UNIVERSITY OF TRAVNIK, FACULTY OF MANAGEMENT AND BUSINESS ECONOMICS

AZAPOVIĆI 439, KISELJAK

BOSNIA AND HERZEGOVINA

www.incohis.com

info@incohis.com

ISBN: 978-625-95551-6-4

EDITORS

- Prof. Dr. Hüseyin TOROS, Istanbul Technical University
- Prof. Dr. Muhamed COSIC, University of Travnik, Bosna and Herzegovina
- Prof.Lecturer Dr. Mustafa OF, Kocaeli University
- Prof.Lecturer İsmail KILIÇASLAN, Kocaeli University

All Rights Reserved
All Responsibilities of The Articles Belong to The Authors

SUPPORTERS

Güngören Municipality

Aleksandër Moisiu University, Albania

Universiteti Bujqësor i Tiranës - UBT, Albania

Uzhhorod National University, Ukraine

University Malaysia Terengganu, Malaysia

İstanbul Technical University Meteorological Research Club, Türkiye

University of Travnik

University of Travnik Faculty of Management and Business Economics

Ekodigitus Center for Sustainability and Digitalization

Dear participants,

INCOHIS 2025 AUTUMN Congress is an internationally recognized academic event. With this congress, where face-to-face and remote participation is supported, you will have the opportunity to present your scientific publications. Our congress, which is attended by respected names in the scientific community, is a candidate congress to bring new horizons to science.

From 11 countries 116 participants applied to the congress. Participants presented their papers for two days in the congress.

We are also grateful to the esteemed participants, our keynote speakers, our referees for their support and contributions to the success of this congress. Thank you for attending our academic event and supporting us.

The INCOHIS congress will be held every year by raising its target higher. It will reach out to wider communities and increase the number of papers and participants.

Any kind of feedback about the congress is very important to us. You can reach our congress from our web page, info@incohis.com e-mail address and official social media accounts.

08.12.2025

INCOHIS ORGANIZING COMMITTEE

KEYNOTE SPEAKERS



Prof.Dr. Mahiboobsab Ahmedhusen Nagarbawadi
Principal ARHAM International institute of Information Security, Pune. India



Prof.Dr. Lyudmyla Symochko
Uzhhorod National University, Ukraine, Coimbra University, Portugal



Prof.Dr. Arbnor Pajaziti
Universiteti i Prishtinës "Hasan Prishtina", Kosova



Prof.Dr. Desire Nizigiyamana Louis
University of Burundi, Burundi



Assoc. Prof. Dr. Zaleha Mohamad,
Universiti Malaysia Terengganu, Malaysia

SCIENCE COMMITTEE

Listed in alphabetical order

- Prof. Dr. Ahmet Duran Şahin, İstanbul Technical University, Türkiye
- Prof. Dr. Ali Deniz, İstanbul Technical University, Türkiye
- Prof. Dr. Ayşe Günsel, Kocaeli University, Türkiye
- Prof. Dr. Engin Özdemir, Kocaeli University, Türkiye
- Prof. Dr. Fatma Çanka Kılıç, Kocaeli University, Türkiye
- Prof. Dr. Flora Merko, Aleksander Moisiu Durres University, Albania
- Prof. Dr. Hanefi Bayraktar, Atatürk University, Türkiye
- Prof. Hiroyuki Ishizaki, Shibaura Institute of Technology, Japan
- Prof. Dr. Hristo Ivanov Katrandzhiev, University of National and World Economy, Bulgaria
- Prof. Dr. Hüseyin Toros, İstanbul Technical University, Türkiye
- Prof. Dr. Hysen Mankolli, Editor of IJEES, Health and Environment Association, U.S.A.
- Prof. Dr. Juan Carlos, Roca University Of Huelva, Spain
- Prof. Dr. Maan T. J. Maaroof, Mousul University, Iraq
- Prof. Dr. Mehmet Demirtaş, Bitlis Eren University, Türkiye
- Prof. Dr. Mehboob Nagarbawdi, Principal ARHAM International institute of Information Security, Pune, India
- Prof. Dr. Muhamed Cosic, University of Travnik, Bosna and Herzegovina
- Prof. Dr. Muhammet Fatih Genç, Kocaeli University, Türkiye
- Prof. Dr. Nardane Yusifova, Azerbaijan National Academy of Sciences, Azerbaijan
- Prof. Dr. Novo Palakalovic, University of East Sarajevo, Bosnia
- Prof. Dr. Olena Demyanyuk, Institute of Agroecology and Environmental Management, Kyiv, Ukraine
- Prof. Dr. Osman Taylan, King Abdulaziz University, Saudi Arabia
- Prof. Dr. Şükrü Dursun, Konya Technical University, Türkiye
- Prof. Dr. Tamara Milenkovic Kerkovic, University of Nis, Serbia
- Assoc. Prof. Dr. Ayşenur Kayabaş Avşar, Çankırı Karatekin University, Türkiye
- Assoc. Prof. Dr. Arben Kambo. Agriculture University of Tirana, Albania
- Assoc. Prof. Dr. Ayşegül Türk, Ankara Haci Bayram Veli University, Türkiye
- Assoc. Prof. Dr. Azeta Tartaraj, Aleksander Moisiu Durres University, Albania
- Assoc. Prof. Dr. Brunela Trebicka, Aleksander Moisiu Durres University, Albania
- Assoc. Prof. Dr. Eda Bezhani, Aleksander Moisiu Durres University, Albania
- Assoc. Prof. Dr. Eda Bozkurt, Atatürk University, Türkiye
- Assoc.Prof.Dr. Edmond Hoxha, Polytechnic University Of Tirana, Albania
- Assoc. Prof. Dr. Emira Kalaj, University of Shkodra "Luigj Gurakuqi", Albania
- Assoc. Prof. Dr. Etleva Dashi. Agriculture University of Tirana, Albania
- Assoc. Prof. Dr. Ercan Arpaz, Kocaeli University, Türkiye
- Assoc. Prof. Dr. Lyudmyla Symochko, Uzhhorod National University, Ukraine
- Assoc. Prof. Dr. Nagip Skenderi, University of Prishtina, Kosovo
- Assoc. Prof. Dr. Natalya Gudkova, The State Ecological Academy, Ukraine
- Assoc. Prof. Dr. Nermin Demirkol, Kocaeli University, Türkiye
- Assoc. Prof. Dr. Taner Erdoğan, Kocaeli University, Türkiye

- Assoc. Prof. Dr. Ylber Aliu, AAB College, Kosovo
- Assoc. Prof. Dr. Samad Rahimi Aghdam, Tabriz University, Iran
- Assoc. Prof. Dr. Seher Uçkun, Kocaeli University
- Assoc. Prof. Dr. Selda Uca, Kocaeli University
- Assist. Prof. Dr. Mazin Nazar Fadhel, Mosul university, Musul, Iraq
- Assist Prof.Dr. Muskan Ramiz Rajjab, KUMM'S Vasantrao Naik college of Arts and Commerce Murud Janjira Dist-Raigad. India
- Assist. Prof. Dr. Berna Kavaz Kındığılı, Atatürk University, Türkiye
- Assist. Prof. Dr. Fatih Sevgi, Selçuk University, Türkiye
- Assist. Prof. Dr. Handan Özçelik Bozkurt, Sinop University, Türkiye
- Assist. Prof. Dr. Larissa Shragina, Odessa I. I. Mechnikov University, Ukraine
- Assist. Prof. Dr. Nuray Aşantuğrul, Amasya University, Türkiye
- Assist. Prof. Dr. Seyil Najimudinova, Kyrgyzstan Türkiye Manas University, Kyrgyzstan
- Assoc. Prof. Dr. Tuncer Gövdeli, Atatürk University, Türkiye
- Assoc. Prof. Dr. Zaleha Mohamad, Universiti Malaysia Terengganu, Malaysia
- Assist. Prof. Dr. Vedat Tümen, Bitlis Eren University, Türkiye
- Assist. Prof. Dr. Vystavkina Daria, Odessa I. I. Mechnikov University, Ukraine
- Assist. Prof. Dr. Yıldırım Karadeniz, Kocaeli University, Türkiye
- Assist. Prof. Dr. Yusuf Budak, Kocaeli University, Türkiye
- PTech. Dr. Isma Rosila, Universiti Malaysia Terengganu, Malaysia
- Phd. Alba Ramallari, Aleksandër Moisiu University Durrës, Albania
- Phd. Alma Zisi, Aleksandër Moisiu University Durrës, Albania
- Phd. Blerina Vrenozi, Tirana University, Albania
- Phd. Daniela Lika, Aleksander Moisiu Durres University, Albania
- PhD. Gülşah Keklik, İstanbul Technical University
- Phd. Irfan Wahyudi, Universitas Airlangga, Indonesia
- Phd. Mirela Alushllari, University of Albania, Albania
- Phd. Jonida Gashi, Aleksander Moisiu Durres University, Albania
- Phd. Olta Nexhipi, Aleksandër Moisiu University Durrës, Albania
- Phd. Violeta Neza, Aleksander Moisiu Durres University, Albania
- Phd. Ariola Harizi, Aleksander Moisiu Durres University, Albania
- Phd. Saeid Shojaei, University of Tabriz, Iran
- Phd. Süleyman Soydaş, Kocaeli University, Türkiye
- Phd. Ada Aliaj, Aleksandër Moisiu University Durrës, Albania
- Phd. Moses M. Solomon, King Fahd University, Saudi Arabia
- Phd. Emma Gurashi Nikolaoy, University Of Patras, Greece
- Phd. Hisham M. Alidrisi, King Abdulaziz University, Saudi Arabia
- Phd. Thawee Numsakulwong, Rajamangala University of Technology Isan, Tayland
- Phd. Reyhan Dadash, Baku Business University, Azerbaijan
- Lecturer Dr. Mustafa Of, Kocaeli University
- Lecturer İsmail Kılıçaslan, Kocaeli University

CONTENTS

ABSTRACTS / POSTERS 1

PRODUCTION OF 1% GLASS FIBER REINFORCED ABS VIA SLA 3D PRINTING AND EVALUATION OF ITS MECHANICAL PROPERTIES 2

MODULAR PRODUCTION OF POST-DISASTER TEMPORARY SHELTERS AS A STUDENT WORKSHOP EXPERIENCE 3

THE IMPACT OF ERP SYSTEMS ON DIGITAL TRANSFORMATION IN SMES 4

GENERATIVE ARTIFICIAL INTELLIGENCE AND EDUCATION 5

EVALUATION OF PHYSICOCHEMICAL PARAMETERS IN MODELLING NITRATE POLLUTION IN SURFACE WATERS 6

THE EFFECT OF ROLLING RESISTANCE COEFFICIENT (RRC) OF TIRES ON ENERGY CONSUMPTION IN N2 CATEGORY ELECTRIC CARGO VAN VEHICLES 7

DETERMINATION OF TECHNOLOGICAL PROPERTIES OF SOME LACTIC ACID BACTERIA ... 8

EFFICACY OF LACTOBACILLUS PLANTARUM AND PEDIOCOCCUS PENTOSACEUS AGAINST FOODBORNE PATHOGENS 9

ASSESSMENT OF THE BIOPROTECTIVE POTENTIAL OF LACTIC ACID BACTERIA (LAB) AGAINST MYCOTOXIGENIC MOLDS IN FOODS 10

EFFECT OF CELL-FREE SUPERNATANTS OF LACTOBACILLUS PLANTARUM AND PEDIOCOCCUS PENTOSACEUS ON THE EXPRESSION OF BIOFILM- AND VIRULENCE-RELATED GENES IN SALMONELLA TYPHIMURIUM 11

DETERMINATION OF FACTORS AFFECTING PROGRAM SETUP TIMES IN PRODUCTION PLANNING USING MACHINE LEARNING METHODS 13

SYNTHESIS AND CHARACTERIZATION OF PHTHALOCYANINE DERIVATIVES CONTAINING FUNCTIONAL GROUPS 14

FILM QUALITY PREDICTION: AN OPTIMIZED MULTIMODAL STACKING APPROACH USING TEXTUAL, VISUAL AND TABULAR DATA 16

INVESTIGATION OF THE EFFECT OF RESISTOR TOLERANCES ON SYSTEM RELIABILITY IN POWER ELECTRONICS CIRCUITS 17

IMPACT OF CAPACITOR TOLERANCES ON RELIABILITY OF POWER ELECTRONICS CIRCUITS 18

COMPARISON OF THE PERFORMANCE OF SWIN TRANSFORMER V2-B AND CNN MODELS IN DIABETIC RETINOPATHY CLASSIFICATION 19

FPGA-BASED DEEP LEARNING NETWORK FOR SUPER-RESOLUTION ENHANCEMENT OF ULTRASOUND IMAGES 20

EXPERIMENTAL EVALUATION OF THE EFFECTS OF RAILWAY TRAFFIC-INDUCED VIBRATIONS ON A HISTORICAL MASONRY STRUCTURE 21

NANO HYDROXYAPATITE-REINFORCED COLLAGEN HYDROLYSATE FILMS FROM LEATHER WASTE WITH IMPROVED WATER BARRIER PERFORMANCE 22

TREND ANALYSIS OF METEOROLOGICAL DROUGHT INDICES (SPI, ASPI AND SPEI) IN BOZCAADA 23

DETERMINATION END EVALUAITON OF RHEOLOGICAL PROPERTIES OF SOLID LUBRICANTS ON CALCIUM GREASES 24

FULL TEXT PAPERS 25

LASTİKLERİN YUVARLANMA DİRENCİ KATSAYISININ (RRC) N2 KATEGORİ ELEKTRİKLİ KARGO VAN ARAÇLARDA ENERJİ TÜKETİMİNE ETKİSİ 26

FİLM KALİTESİ TAHMİNİ: METİN, GÖRSEL VE TABLO VERİLERİNİ KULLANARAK OPTİMİZE EDİLMİŞ ÇOK MODLU YIĞINLAMA YAKLAŞIMI 31

GÜÇ ELEKTRONİĞİ DEVRELERİNDE DİRENÇ TOLERANSLARININ SİSTEM GÜVENİLİRLİĞİ ÜZERİNDEKİ ETKİSİNİN İNCELENMESİ 39

KONDANSATÖR TOLERANSLARININ GÜÇ ELEKTRONİĞİ DEVRELERİNİN GÜVENİLİRLİĞİNE ETKİSİNİN İNCELENMESİ 46

COMPARISON OF THE PERFORMANCE OF SWIN TRANSFORMER V2-B AND CNN MODELS IN DIABETIC RETINOPATHY CLASSIFICATION 53

NANO HYDROXYAPATITE-REINFORCED COLLAGEN HYDROLYSATE FILMS FROM LEATHER WASTE WITH IMPROVED WATER BARRIER PERFORMANCE 62

ABSTRACTS / POSTERS

The abstract fields of the papers that have met all the conditions of the INCOHIS 2025 AUTUMN congress as abstract, poster and full text will be shown on the following pages. In addition, the full texts of the papers that have been applied as full text are available on the following pages.

PRODUCTION OF 1% GLASS FIBER REINFORCED ABS VIA SLA 3D PRINTING AND EVALUATION OF ITS MECHANICAL PROPERTIES

BURAK ÖZEL
Bursa Technical University, Faculty Of Engineering, Metallurgical And Materials Engineering
burakkozelll@gmail.com

CAN EKİNCİ
Bursa Technical University, Faculty Of Engineering, Polymer Engineering
cannekincii1@gmail.com

Assoc. Prof. Dr. Doç. Dr. ÖMER YUNUS GÜMÜŞ
Bursa Technical University, Faculty Of Engineering, Polymer Engineering
omer.gumus@btu.edu.tr

Assoc. Prof. Dr. Doç. Dr. FATMA NUR PARIN
Bursa Technical University, Faculty Of Engineering, Polymer Engineering
nur.parin@btu.edu.tr

Abstract
In this study, composite specimens were fabricated by incorporating 1 wt.% of 3 mm long glass fiber reinforcement into acrylonitrile butadiene styrene (ABS)-based polymer material using stereolithography (SLA) 3D printing. The aim of the study is to investigate the effect of low fiber content on the mechanical performance of parts produced via 3D printing. The glass fibers were homogeneously dispersed in the resin through mechanical mixing, and the specimens were subsequently produced using the SLA method. Tensile and flexural tests were conducted on both pure ABS and 1% glass fiber-reinforced composite specimens. The results indicated that the low fiber content did not provide a significant improvement in tensile strength or flexural modulus of the material. Weak fiber–matrix interfacial bonding and low fiber volume fraction were identified as the main reasons for this outcome. In conclusion, the incorporation of a low amount of glass fiber in ABS-based composites produced by SLA had a limited effect on en

Keywords: Abs, Glass Fiber, Composite Material, 3d Printing, Flexural Test Stereolithography, Tensile Test,

MODULAR PRODUCTION OF POST-DISASTER TEMPORARY SHELTERS AS A STUDENT WORKSHOP EXPERIENCE

Lecturer YASEMİN AKCAKAYA
İstanbul Esenyurt University, Faculty of Architecture and Engineering, Interior Architecture
yaseminakcakaya@esenyurt.edu.tr

Assistant CAN BALDAN
İstanbul Esenyurt University, Faculty of Architecture and Engineering, Interior Architecture
canbaldan@esenyurt.edu.tr

Assist. Prof. Dr. ECE CANTEMİR
İstanbul Gelişim University, Faculty Of Fine Arts, Interior Architecture And Environmental Design
ecantemir@gelisim.edu.tr

Abstract
Across the world, numerous natural disasters such as earthquakes, floods, storms, and tsunamis occur, leaving both material and emotional impacts on societies. These disasters endanger human life and property and often render living spaces unusable. As a result, there arises a need for temporary and permanent shelter areas to accommodate individuals who have lost their homes. Temporary shelters established to prevent people from being left without accommodation after disasters may, in some cases, evolve into permanent housing solutions. The rapid installation of these shelters, their resistance to external factors, ease of storage, modularity, environmental friendliness, sustainability, user-centered adaptability, and provision of comfort are essential parameters in terms of quality. In this study, the design approaches developed by Interior Architecture students to address the issue of temporary housing are examined. The findings are expected to shed light on future studies and contribute to the development of effective post-disaster shelter solutions.

Keywords: Natural Disaster, Temporary Shelter, Modular Design, Interior Architecture

THE IMPACT OF ERP SYSTEMS ON DIGITAL TRANSFORMATION IN SMES

HATİCE KÜBRA KILIÇASLAN
Kocaeli University, Faculty Of Engineering, Computer Engineering
kubrakilicaslann@gmail.com

Abstract
In the modern competitive environment, achieving sustainable growth requires businesses to adapt effectively to digital transformation. Digital transformation is not merely a technological upgrade but a comprehensive change that reshapes organizational structures and decision-making processes. Within this framework, Enterprise Resource Planning (ERP) systems have emerged as a critical tool that integrates core business functions—such as finance, production, human resources, inventory management, and customer relations—into a unified digital platform, enabling seamless information flow and operational transparency. This study examines the impact of ERP systems on small and medium-sized enterprises (SMEs). Through an extensive literature review, the research analyzes ERP's contributions to business performance, data integrity, operational efficiency, and strategic decision-making. It also explores the challenges SMEs face during ERP adoption, including cost management, employee adaptation, and system integration. The findings highlight that ERP systems are not only technological solutions but also strategic components that enhance digital maturity and organizational competitiveness. The results indicate that effectively implemented ERP systems accelerate the digital transformation of SMEs by improving data-driven management, strengthening internal coordination, and increasing operational efficiency. Therefore, ERP can be regarded as a strategic investment that empowers SMEs to achieve long-term sustainability and gain a competitive edge in the evolving digital economy.

Keywords: Transformation, Erp System, Artificial Intelligence

GENERATIVE ARTIFICIAL INTELLIGENCE AND EDUCATION

BUSE KÜÇÜKGÖL
Sakarya University, Graduate School Of Business, Management Information Systems
buse.kucukgol@ogr.sakarya.edu.tr

Assist. Prof. Dr. TUĞBA KOÇ
Sakarya University, Faculty Of Business Administration, Management Information Systems
tugbakoc@sakarya.edu.tr

Abstract
The aim of this study is to review the existing literature on the usage of generative artificial intelligence in the education and to reveal the trends. Within the scope of the study, TR Index and Google Scholar databases were searched using the keywords ‘generative artificial intelligence’ and ‘education’. Of the total 43 studies found, 13 articles were selected in terms of their content and scope appropriateness. The analyses revealed that generative artificial intelligence offers significant contributions to the educational environment in various aspects, such as personalised learning, increased efficiency, and time and resource savings. However, while some studies addressed niche types of generative artificial intelligence; others discussed the general role of artificial intelligence in education. This finding indicates that the topic of generative artificial intelligence is still in its developmental stage in the literature and that the field requires more in-depth studies. The research aims to provide a guiding framework for future studies by evaluating the orientations of existing studies from a systematic perspective.

Keywords: Generative Artificial Intelligence, Education, Artificial Intelligence Applications

EVALUATION OF PHYSICOCHEMICAL PARAMETERS IN MODELLING NITRATE POLLUTION IN SURFACE WATERS

HATİCE KANBERİZ
Dokuz Eylül University, Institute Of Science, Statistics
hatice.kanberiz@ogr.deu.edu.tr

Assoc. Prof. Dr. ÖZGÜL VUPA ÇİLENGİROĞLU
Dokuz Eylül University, Institute Of Science, Statistics
ozgul.vupa@deu.edu.tr

Abstract
Among the existing sectors in Turkey (agriculture, industry, drinking water, tourism, etc.), agricultural irrigation accounts for 74% of water consumption. 97.5% of the total amount of water on Earth is found as salt water in oceans and seas, and 2.5% is found as fresh water in rivers and lakes. Approximately 30% of freshwater consists of groundwater, while the remaining 0.4% consists of atmospheric water and surface water. This study aims to determine the nitrate pollution levels in agricultural surface waters of Erzurum province, Türkiye, and to demonstrate the basic relationships between nitrate measurement values and physicochemical parameters using data between 2022 and 2024. For this purpose, “Nitrate”, “Total Phosphorus”, “Total Nitrogen”, “Orthophosphate”, “pH”, “Temperature”, “Conductivity” and “Oxygen” values were taken as data from 78 surface stations. According to the descriptive statistics and correlation analysis results, the positive relationships between nitrate, orthophosphate and total nitrogen clearly show the effect of agricultural pollution by showing that they are fed by a common external source (fertilization, etc.). The inverse relationship between orthophosphate and oxygen may indicate a process that may cause depletion of dissolved oxygen, especially as a result of eutrophication (algal bloom). It was also found within the scope of the study that the physical parameters pH, temperature and oxygen did not show very strong connections with chemical charges.

Keywords: Nitrate Pollution, Surface Waters, Physicochemical Parameters

THE EFFECT OF ROLLING RESISTANCE COEFFICIENT (RRC) OF TIRES ON ENERGY CONSUMPTION IN N2 CATEGORY ELECTRIC CARGO VAN VEHICLES

Engineer AHMET SERDAR SERTER
Koluman Otomotİv EndÜstrİ A.Ş., Engineering, R&d
serdar.serter@koluman.com

Abstract
Cargo van vehicles inherently have high aerodynamic drag due to their height and width. In this study, the energy consumption of an N2 category electric cargo van was compared by using tires with different rolling resistance coefficients (RRC) within the limit values specified on the European tire label. At the same time, the effect of different RRC values on vehicle efficiency was observed. Based on the classification table in Regulation (EU) 2020/740 on the labeling of tires with respect to fuel efficiency and other parameters, simulations were performed in the VECTO (Vehicle Energy Consumption Calculation Tool) program using 215/75 R17.5 tires with rolling resistance coefficients (RRC) of 6.1 N/kN and 7.0 N/kN for various road scenarios of the electric van. According to the analysis results, the tire with an RRC of 6.1 N/kN showed an energy consumption of 0.6588 kWh/km and a zero CO_2 emission driving range of 38.3 km, while the tire with an RRC of 7.0 N/kN showed an energy consumption of 0.6724 kWh/km and a zero CO_2 emission driving range of 37.5 km. Based on the analysis, the tire with an RRC of 6.1 N/kN provided 2.06% better energy efficiency and a 2.1% longer zero CO_2 emission range compared to the tire with an RRC of 7.0 N/kN. The results indicate that reducing the rolling resistance coefficient positively affects the energy consumption and zero CO_2 emission driving range of electric cargo vans.

Keywords: Vecto, Rrc, Rolling Resistance, Emission, Energy Consumption, Zero Co_2 Emission

DETERMINATION OF TECHNOLOGICAL PROPERTIES OF SOME LACTIC ACID BACTERIA

FATMA AYLİN SEZER
Ankara University, Faculty Of Science, Biology
fasezer@ankara.edu.tr

Prof. Dr. ÖZLEM OSMANAĞAOĞLU
Ankara University, Faculty Of Science, Biology
osmanaga@ankara.edu.tr

Abstract
This study examines the technological and probiotic properties of lactic acid bacteria (LAB) strains obtained from traditionally produced homemade cheeses collected in the Gaziantep, Şanlıurfa and Mardin provinces of Turkey. Six isolates were obtained and screened for antibacterial activity against various indicator bacteria. Several of the strains exhibited strong inhibitory effects, suggesting potential probiotic functionality. The selected isolates were characterized in terms of their acidification capacity, proteolytic and decarboxylase activities, and resistance to simulated gastrointestinal conditions, including low pH, bile salts, pepsin and pancreatin. Their autoaggregation, coaggregation and adhesion to Caco-2 cells were evaluated to assess their potential for intestinal colonization. The isolates demonstrated high survival rates in acidic and bile conditions, as well as notable aggregation and adhesion properties, indicating their potential as probiotics. Molecular identification using 16S rDNA sequencing confirmed that all isolates belonged to the strain Pediococcus acidilactici. This strain is known for its ability to produce bacteriocins and improve the safety and quality of fermented dairy products. The isolates identified in this study exhibited the technological features that are desirable in starter cultures, such as acid production, proteolytic activity and antibacterial effects against common foodborne pathogens. The results suggest that P. acidilactici strains isolated from traditional Turkish cheeses have probiotic and technological properties that could be used to develop novel starter cultures for the dairy industry. This research highlights the importance of traditional fermentation practices as a valuable source of unique, functionally significant microbial strains that contribute to food biotechnology and public health.

Keywords: Lactic Acid Bacteria, Pediococcus Acidilactici, Probiotic, Starter Culture, Traditional Cheese, Antibacterial Activity

EFFICACY OF LACTOBACILLUS PLANTARUM AND PEDIOCOCCUS PENTOSACEUS AGAINST FOODBORNE PATHOGENS

Prof. Dr. ÖZLEM OSMANAĞAOĞLU
Ankara University, Faculty Of Science, Biology
osmanaga@ankara.edu.tr

MOHAMMED BAHRAM KHORSHEED ALDAWOODI
Ankara University, Faculty Of Science, Biology
mbkiraq@yahoo.com

ASİYE NUR KARACA
Ankara University, Faculty Of Science, Biology
ankaraca@ankara.edu.tr

FATMA AYLİN SEZER
Ankara University, Faculty Of Science, Biology
fasezer@ankara.edu.tr

ZAINAB HUSSEIN FADHIL FADHIL
Ankara University, Faculty Of Science, Biology
zeynep.bayraktar81@gmail.com

Abstract
This study aims to evaluate the inhibitory effects of two strains of lactic acid bacteria (LAB), Pediococcus pentosaceus and Lactobacillus plantarum, against a number of food-borne pathogenic bacteria. Lactic acid bacteria are known for their health properties and benefits as natural antagonists of harmful bacteria, making them important in the food and pharmaceutical industries. Planktonic cells, biofilms, and cell-free supernatants of these two strains were selected against eight pathogenic bacteria, including *Listeria monocytogenes, Staphylococcus aureus, Bacillus subtilis, Enterococcus faecalis, Enterococcus faecium, Escherichia coli, Salmonella* Typhimurium, and *Pseudomonas aeruginosa*. The antibacterial activity of the supernatants was determined using microdilution techniques and the plate spread method, while the crystal violet test was used to measure the effect of planktonic cells on the biofilms of pathogens. The results showed that 48 hours of incubation was optimal for biofilm formation in both strains. L. plantarum showed a higher ability to produce biofilms compared to P. pentosaceus. Both strains showed a clear ability to inhibit the growth of pathogenic bacteria, with P. pentosaceus being more effective against B. subtilis and S. Typhimurium, while L. plantarum was more effective against E. coli and P. aeruginosa. The results also showed that both strains have a strong ability to auto-aggregate and co-aggregate with other bacteria, with the highest aggregation rates recorded with E. faecium and P. aeruginosa. Scanning electron microscopy (SEM) analysis revealed clear differences in the structure of the biofilms, with P. pentosaceus forming compact, regular biofilms, while L. plantarum formed irregular and more dispersed biofilms. These results show that both P. pentosaceus and L. plantarum can play effective roles in controlling food pathogens through the production of biofilms and antibacterial compounds. Therefore, they can be considered promising candidates for use in the food industry as natural anti-pathogenic agents.

Keywords: Probiotic, Foodborne, Antagonistic, Antiadhesion, Sem, Cfs, Pathogenic Bacteria

ASSESSMENT OF THE BIOPROTECTIVE POTENTIAL OF LACTIC ACID BACTERIA (LAB) AGAINST MYCOTOXIGENIC MOLDS IN FOODS

Prof. Dr. ÖZLEM OSMANAĞAOĞLU
Ankara University, Faculty Of Science, Biology
osmanaga@ankara.edu.tr

ZAINAB HUSSEIN FADHIL FADHIL
Ankara University, Faculty Of Science, Biology
zeynep.bayraktar81@gmail.com

ASİYE NUR KARACA
Ankara University, Faculty Of Science, Biology
ankaraca@ankara.edu.tr

FATMA AYLİN SEZER
Ankara University, Faculty Of Science, Biology
fasezer@ankara.edu.tr

Abstract
Fungal (mold) contamination of food products is a significant global problem, leading to both economic losses and public health concerns. Mold growth negatively impacts food quality by causing deterioration in the appearance, odor, taste, and texture of products. However, some mold species are capable of producing mycotoxins (e.g., aflatoxin, ochratoxin A, fumonisin, and patulin), which can be toxic to humans and animals. Mycotoxins pose a serious risk to food safety due to their resistance to many processing conditions, such as high temperatures and pH changes. While physical (drying, irradiation, etc.) and chemical (preservatives such as sorbate and propionate) methods are widely used to prevent mold growth, consumer interest in natural and additive-free foods has brought biological preservation approaches to the forefront. In this regard, lactic acid bacteria (LAB), a member of the natural microflora, are attracting attention as alternative biopreservatives due to their antimicrobial and, in particular, antifungal properties. In this study, we evaluated the antifungal activities of Lactobacillus, Bifidobacterium, and Pediococcus isolates from our laboratory against mold species such as Aspergillus, Fusarium, and Candida. Various thermal, enzymatic, and pH treatments were used to characterize the antifungal compounds in LAB supernatants, and the stability of the antifungal compounds was assessed. Furthermore, the organic acid profile and protein structure produced by the LAB isolates were analyzed. These findings support the potential use of LAB strains as natural food preservatives and contribute to the development of safe, high-quality products in the food industry.

Keywords: Lactic Acid Bacteria, Antifungal Activity, Mycotoxin, Biopreservation, Cheese Model

EFFECT OF CELL-FREE SUPERNATANTS OF LACTOBACILLUS PLANTARUM AND PEDIOCOCCUS PENTOSACEUS ON THE EXPRESSION OF BIOFILM- AND VIRULENCE-RELATED GENES IN SALMONELLA TYPHIMURIUM

Prof. Dr. ÖZLEM OSMANAĞAOĞLU
Ankara University, Faculty Of Science, Biology
osmanaga@ankara.edu.tr

MOHAMMED BAHRAM KHORSHEED ALDAWOODI
Ankara University, Faculty Of Science, Biology
mbkiraq@yahoo.com

ZAINAB HUSSEIN FADHIL FADHIL
Ankara University, Faculty Of Science, Biology
zeynep.bayraktar81@gmail.com

ASİYE NUR KARACA
Ankara University, Faculty Of Science, Biology
ankaraca@ankara.edu.tr

FATMA AYLİN SEZER
Ankara University, Faculty Of Science, Biology
fasezer@ankara.edu.tr

Abstract
In this study, the results of gene expression analysis using (qRT-PCR) showed that treatment of *Salmonella* Typhimurium strains with cell free culture supernatan(CFCS) from *Pediococcus pentosaceus and Lactobacillus plantarum* bacteria led to a significant change in the gene expression levels of a number of genes associated with biofilm formation and virulence. After performing RNA purity checks and converting them to cDNA, the reference gene gyrA was used to calibrate the data. The results showed that all target genes, namely invA, csgD, rpoS, hilA, spiC, adrA, and fliF, exhibited a decrease in gene expression levels after the application of CFCS extracts compared to the control strain that was not treated. The genes responsible for biofilm formation (csgD and adrA) decreased significantly, indicating that the CFCS directly affected the ability of S. Typhimurium to form and stabilize its biofilm layer. This result is very important because the biofilm is one of the most important resistance factors that help bacteria survive in extreme environments and resist antibacterial agents. As for the virulence-associated genes (invA, rpoS, hilA, spiC, and fliF), they also showed a significant decrease in gene expression levels, indicating that P. pentosaceus and L. plantarum extracts not only inhibit biofilm formation but also reduce the ability of pathogenic bacteria to adhere to host cells, invade them, and cause infection. The comparison between the two extracts also showed that the P. pentosaceus extract was more effective in inhibiting the gene expression of the target genes compared to the L. plantarum extract, especially for the csgD, invA, and adrA genes, indicating that the active substances in the P. pentosaceus extract have a higher ability to disrupt the regulatory systems responsible for biofilm formation and virulence in S. Typhimurium. Overall, these results show that CFCS of P. pentosaceus and L. plantarum have an effective ability to inhibit the genes responsible for virulence and biofilm formation in S. Typhimurium. This suggests the possibility of using these strains as anti-biofilm

agents or as natural alternatives to antibiotics in the food and medical industries, especially in the field of combating foodborne pathogenic bacteria.

Keywords: Salmonella Typhimurium, Pediococcus Pentosaceus, Lactobacillus Plantarum, (cfcs), Qrt-pcr, Gene Expression, Biofilm Formation, Virulence Factors, Antibiofilm Activity, Probiotic Bacteria

DETERMINATION OF FACTORS AFFECTING PROGRAM SETUP TIMES IN PRODUCTION PLANNING USING MACHINE LEARNING METHODS

ADEM KUŞ
Dokuz Eylül University, Institute Of Science And Technology, Data Science
ademkus1996@gmail.com

Assoc. Prof. Dr. ÖZGÜL VUPA ÇİLENGİROĞLU
Dokuz Eylül University, Institute Of Science And Technology, Statistics
ozgul.vupa@deu.edu.tr

Abstract
In this study, production-related data obtained from the corporate ERP/MES infrastructure (SAP and Doruk) of an industrial fastener manufacturing facility operating in İzmir, Turkey, covering the years 2014–2025, were utilized to identify the factors influencing program setup time and to develop a predictive model to support production planning decisions. Program setup time is defined as the duration between the completion of production for the previous part and the point at which the machine becomes ready to resume mass production with the next part. Both statistical methods and machine learning models were employed for this purpose. The dataset used in the study belongs to four press machines of the same model, selected to provide a homogeneous analysis environment due to their processing of similar and identical product groups. Following data preprocessing, descriptive statistics, correlation analyses, regression models, and machine learning approaches (Linear Regression, Random Forest, XGBoost, and Artificial Neural Networks) were applied. Comparison metrics indicated that the Random Forest model achieved the highest predictive performance, followed by XGBoost. In contrast, the lower performance of the linear regression model was attributed to its limited ability to capture nonlinear and interaction-based relationships among variables. The results revealed that variables such as metric change between the previous and the new product, piercing pin diameter difference, transitions in product types, time elapsed since the last production, raw material/diameter relationship, and operator competency exhibited statistically significant effects on program setup time.

Keywords: Setup Time, Machine Learning, Production Planning, Data Analytics, Feature Engineering

SYNTHESIS AND CHARACTERIZATION OF PHTHALOCYANINE DERIVATIVES CONTAINING FUNCTIONAL GROUPS

YAĞMUR ZEYNEP YURDAKUL
İstanbul Technical University, Faculty Of Arts And Sciences, Chemistry
yurdakul.yagmur.zeynep@gmail.com

Assoc. Prof. Dr. MUKADDES ÖZÇEŞMECİ
İstanbul Technical University, Faculty Of Arts And Sciences, Chemistry
selcukoglu@itu.edu.tr

Prof. Dr. ESİN HAMURYUDAN
İstanbul Technical University, Faculty Of Arts And Sciences, Chemistry
esin@itu.edu.tr

Abstract
Phthalocyanines (Pcs), owing to their conjugated 18-π electron systems, high thermal stability, and remarkable optical properties, are among the most important tetrapyrrole derivatives with a wide range of applications such as liquid crystals, optical data storage, laser dyes, catalysis, and photodynamic therapy [1,2]. The planar and stable tetrapyrrole ring systems of phthalocyanines allow the synthesis of new compounds for various applications through the introduction of novel substituents and the modification of the central metal ion.

Pyrene (Py) derivatives are alternative planar polycyclic aromatic hydrocarbon systems. The strong π-electron delocalization within the pyrene structure endows it with superior photophysical and photochemical properties. Therefore, in recent years, researchers have incorporated the pyrene moiety into their studies to fulfill specific functions in various scientific fields. Due to its high quantum yield and long fluorescence lifetime, pyrene is one of the most popular fluorescent chromophores used in photochemical applications, and its derivatives are also regarded as valuable molecular probes in fluorescence spectroscopy [3–5].

Thanks to their many outstanding properties, both phthalocyanines and pyrenes are considered promising candidate molecules for various applications. Although each of these functional units has been extensively investigated individually, studies combining both remain quite limited. In this study, the synthesis and characterization of a tetra-substituted zinc phthalocyanine compound functionalized with pyrene groups through alkinyl linkers were successfully carried out.

Keywords: Phtalocyanine (pc), Pyrene (py), Synthesis

Acknowledgements

This work was supported by Istanbul Technical University─ Scientific Research Projects Unit (ITU-BAP) [Project Numbers: 43768 and 44243].

References

[1] N. B. McKeown, Phthalocyanine materials: synthesis, structure and function (1998) (No. 6). Cambridge university press.
[2] V. N. Nemykin, E. A. Lukyanets, Synthesis of substituted phthalocyanines, ARKIVOC: Online J. Org. Chem. (2010)

[3] S. Kagatikar, D. Sunil, D. Kekuda, M. N. Satyanarayana, S. D. Kulkarni, Y. N. Sudhakar, A. K. Vatti, A. Sadhanala, Materials Chemistry and Physics, 293 (2023) 126839.
[4] İ. Özceşmeci, A. Gelir, A. Gül, Dyes and Pigments, 92(3) (2012) 954-960.
[5] S. Sürgün, Y. Arslanoğlu, E. Hamuryudan, Dyes and Pigments, 100 (2014) 32-40.

FILM QUALITY PREDICTION: AN OPTIMIZED MULTIMODAL STACKING APPROACH USING TEXTUAL, VISUAL AND TABULAR DATA

TAYFUN DURMUŞ
Kocaeli University, Institute Of Science And Technology, Software Engineering
tayfundurmus23@gmail.com

Assoc. Prof. Dr. HAKAN GÜNDÜZ
Kocaeli University, Institute Of Science And Technology, Software Engineering
hakan.gunduz@kocaeli.edu.tr

Abstract
This study's objective is to develop a multimodal machine learning model for predicting film quality (a critical regression problem) by integrating textual, visual, and tabular features to evaluate performance (R^2). Various feature extraction engines (CLIP, mpnet, etc.), preprocessing strategies, and model architectures were analyzed. A 9,915 film dataset from TMDB was used. The effect of filtering by vote count was investigated. For feature extraction, textual data used all-mpnet-base-v2, visual data used clip-ViT-B-32, and five key tabular features (e.g., popularity, vote_count) were employed. The impact of feature selection (SelectKBest) and scaling (StandardScaler) on performance was also analyzed. The final model is based on a StackingRegressor (meta-model: RidgeCV) that combines LightGBM, XGBoost, and CatBoost models, each optimized via RandomizedSearchCV over the filtered multimodal dataset. On the filtered dataset (≥ 400 votes), ablation analysis revealed a notable visual signal (CLIP $R^2 \approx 0.21$), while the final optimized stacking model combining all features achieved a test $R^2 = 0.6027$. This study confirms tabular metadata is the dominant signal. However, textual and poster data processed with powerful encoders (all-mpnet-base-v2, clip-ViT-B-32) contributed unique information not in tabular data alone, enhancing model performance. The highest success was achieved through the synergy of (1) data filtering (≥ 400 votes), (2) effective encoders (clip-ViT-B-32), and (3) optimized model stacking. This methodology successfully explains 60.2% of the variance in film quality.

Keywords: Film Quality Prediction, Multimodal Regression, Stacking, Clip, S-bert, R^2

INVESTIGATION OF THE EFFECT OF RESISTOR TOLERANCES ON SYSTEM RELIABILITY IN POWER ELECTRONICS CIRCUITS

Assist. Prof. Dr. MURAT DEMİR
İzmir Bakırçay University, Faculty Of Engineering And Architecture, Electrical-electronics Engineering
murat.demir@bakircay.edu.tr

Abstract
The present study employs a quantitative research methodology to investigate the effect of resistance tolerances on system reliability in power electronics circuits. Despite their frequent categorization as non-critical passive components, variations in manufacturing tolerances have the capacity to exert an indirect influence on circuit operating points, thereby inducing substantial alterations in the overall system failure rate. In this context, three different tolerance scenarios for resistor components were compared: minimum (±1%), nominal (tolerance neglected), and maximum (±10%). The comparison was made using a component stress model based on MIL-HDBK-217F standards. The calculations yielded a system failure rate of 3.3685 FPMH and an estimated lifetime value of 296,868 hours for the minimum tolerance scenario. In the maximum tolerance scenario, the failure rate increased to 3.5618 FPMH, while the lifetime value decreased to 280,757 hours. In the nominal case, the failure rate was calculated as 3.4646 FPMH, and the estimated lifetime value was 288,634 hours. A 5.74% disparity in failure rate and a 16,111-hour discrepancy in lifetime were identified between the minimum and maximum tolerance scenarios. The findings of this study demonstrate that even changes in resistance tolerance alone can have a measurable impact on the reliability indicators of the system. While resistance components do not constitute the primary source of failure in the system, in applications such as LED driver circuits characterized by high production volumes and extended operating times, these discrepancies assume economic and technical significance in terms of the overall reliability of the system.

Keywords: Power Electronics, Reliability Analysis, Resistor Tolerance, Mil-std-217f, Failure Rate Prediction, Led Driver Circuits

IMPACT OF CAPACITOR TOLERANCES ON RELIABILITY OF POWER ELECTRONICS CIRCUITS

Assist. Prof. Dr. MURAT DEMİR
İzmir Bakırçay University, Faculty Of Engineering And Architecture, Electrical-Electronics Engineering
murat.demir@bakircay.edu.tr

Abstract
In power electronic systems, component manufacturing tolerances can cause deviations from nominal values, leading to shifts in circuit operating points and reliability metrics over time. This effect is particularly critical for capacitors used in LED driver circuits, where filtering and energy storage functions are directly influenced by tolerance variations. In this study, the impact of capacitor tolerance bands on system-level reliability was evaluated using the MIL-HDBK-217F part stress method. Three tolerance scenarios (minimum tolerance, nominal, and maximum tolerance) were defined based on manufacturer tolerance codes. Failure rate calculations were performed by isolating capacitor tolerance effects, while other components were kept at nominal values. The results revealed that the total system failure rate varied from 3.4393 FPMH (minimum tolerance) to 3.4872 FPMH (maximum tolerance), corresponding to an approximately 1.38% increase in failure rate and nearly 4,000 hours reduction in lifetime. Although this difference appears moderate, it can result in significant reliability and cost impacts in long-lifetime industrial lighting systems. This study highlights the importance of considering capacitor tolerances as a reliability-critical design parameter. Selecting tighter tolerance components can enhance system lifetime and reduce maintenance frequency, providing a practical decision-making framework for reliability-oriented LED driver design.

Keywords: Power Electronics, Reliability Analysis, Capacitor Tolerance, Mil-std-217f, Failure Rate Prediction, Led Driver Circuits

COMPARISON OF THE PERFORMANCE OF SWIN TRANSFORMER V2-B AND CNN MODELS IN DIABETIC RETINOPATHY CLASSIFICATION

Lecturer EBUBEKİR AKKUŞ
Adnan Menderes University, Germencik Yamantürk Vocational School, Department Of Electronics And Automation
ebubekir.akkus@adu.edu.tr

Prof. Dr. UFUK BAL
Osmaniye Korkut Ata University, Faculty Of Engineering And Natural Sciences, Department Of Electrical And Electronics Engineering
ufukbal@osmaniye.edu.tr

Assistant KÜRŞAD KOCAİSPİR
Osmaniye Korkut Ata University, Faculty Of Engineering And Natural Sciences, Department Of Electrical And Electronics Engineering
kursadkocaispir@osmaniye.edu.tr

Abstract
Diabetic retinopathy (DR) is an eye disease that can cause vision loss if left untreated. However, with early detection and treatment, vision loss can be prevented. With the increase in artificial intelligence studies in recent years, research in medical image classification has also become widespread. Different deep learning methods are used to detect and classify DR. In this study, the DR classification performances of convolutional neural network (CNN)-based models and transformer-based models, which are widely used for DR classification, are investigated, and the obtained results are presented. For this purpose, five different pre-trained CNN models and a transformer model called Swin Transformer V2-B were trained and tested using the APTOS2019 dataset. According to the obtained results, the Swin Transformer V2-B model not only yielded higher accuracy with a test accuracy of 83.22% compared to the CNN models used in the study, but also provided significant improvements in precision, recall, and F1 score metrics.

Keywords: Swin Transformer V2-b, Cnn, Diabetic Retinopathy, Image Classification

FPGA-BASED DEEP LEARNING NETWORK FOR SUPER-RESOLUTION ENHANCEMENT OF ULTRASOUND IMAGES

OĞUZ KAAN ULUIŞIK
Gazi University, Institute of Science, Electrical And Electronics Engineering
oguzkaan.uluisik@gazi.edu.tr

Prof. Dr. HASAN ŞAKİR BİLGE
Gazi University, Faculty Of Engineering, Electrical And Electronics Engineering
bilge@gazi.edu.tr

Abstract
Today, medical imaging systems play a crucial role in diagnosis and treatment processes. Among these systems, ultrasound imaging is widely used due to its non-ionizing nature, low cost, and real-time operation capability. However, ultrasound images often suffer from low resolution, low contrast, and various types of noise, which lead to loss of structural details and reduced diagnostic accuracy. In particular, speckle noise, shadowing, and random noise significantly degrade image quality. Several studies in the literature have focused on enhancing ultrasound image quality through filtering and interpolation-based methods. Although these traditional techniques can operate in real time due to their low computational complexity, they are typically effective for specific noise types and fail to maintain consistent performance under varying noise conditions. In recent years, deep learning-based approaches—especially convolutional neural networks (CNNs)—have shown remarkable success in learning structural relationships within images, effectively reducing noise while preserving important details. In this study, a CNN-based deep learning model was developed to enhance low-resolution and noisy ultrasound images. The proposed model was trained on images containing speckle, white, salt-and-pepper, and shadow noise types, aiming to achieve stable and robust performance under diverse imaging conditions. Experimental results demonstrate that the model effectively suppresses noise and preserves structural features comparable to high-resolution ground-truth images. To achieve real-time operation and reduce power consumption, the trained model was implemented on an FPGA platform. The FPGA-based implementation provided high processing efficiency through parallel computation and demonstrated the system's feasibility for clinical applications. This study presents one of the few implementations of a deep learning-based ultrasound image enhancement model on FPGA hardware. The proposed approach contributes significantly to both engineering and medical fields by combining deep learning's high performance with the efficiency and practicality of hardware-based systems. Acknowledgement This study was supported by the TÜBİTAK ARDEB 1001 Research Project numbered 122E140.

Keywords: Ultrasound, Super-resolution, Noise Reduction, Fpga, Deep Learning Network

EXPERIMENTAL EVALUATION OF THE EFFECTS OF RAILWAY TRAFFIC-INDUCED VIBRATIONS ON A HISTORICAL MASONRY STRUCTURE

Assist. Prof. Dr. ÇAĞLA ŞEKERCİ
Doğuş University, Vocational School, Construction Technology
csekerci@dogus.edu.tr

BAŞAK BODUROĞLU YAZICI
Portneo Engineering Inc., -, -
basak@portneo.com

Assoc. Prof. Dr. ERDEM DAMCI
İstanbul University - Cerrahpaşa, Faculty Of Engineering, Civil Engineering
edamci@iuc.edu.tr

Abstract
In this study, the structural effects of railway traffic-induced vibrations were evaluated on a historical masonry building located approximately 3 meters from the railway line. A total of 18 vibration records were collected using seismic-grade accelerometers placed on the basement, ground, first, and roof floors of the building, measuring in three directions. The acceleration–time data were processed using a third-order Butterworth band-pass filter. For each record, the peak particle acceleration and peak particle velocity components were calculated. In the vibration records where the highest instantaneous velocities were observed, the vibration velocities were examined in the frequency domain using the spectrum method recommended in DIN 4150-3 (2016) standard, and the maximum velocity amplitudes were determined. The evaluations were based on the velocity limits specified in BS 7385-2 (1993) and DIN 4150-3 (2016) standards, and it was observed that all measured vibration levels remained below these limits. The results indicate that railway traffic did not cause vibration effects exceeding cosmetic or minor damage thresholds on the investigated structure. This study highlights the significance of field measurements in assessing vibration-induced damage risks to historical buildings.

Keywords: Vibration Measurement, Masonry Buildings, Railway-induced Vibration, Particle Velocity, Dynamic Effect

NANO HYDROXYAPATITE-REINFORCED COLLAGEN HYDROLYSATE FILMS FROM LEATHER WASTE WITH IMPROVED WATER BARRIER PERFORMANCE

LEVENT İNANÇ
Ege University, Faculty Of Engineering, Department Of Leather Engineering
leventinanc@gmail.com

Prof. Dr. BUĞRA OCAK
Ege University, Faculty Of Engineering, Department Of Leather Engineering
bugra.ocak@ege.edu.tr

Abstract
The tannery industry faces a significant challenge in sustainably managing solid waste, as the large amounts of hazardous materials it generates—particularly collagen-rich leather fiber residues such as trimming waste—can be valorized by incorporation into film production, thereby mitigating environmental pollution. At the same time, increasing awareness of the environmental impact of petroleum-based plastics has led to heightened research interest in bioactive and biodegradable packaging system. Collagen hydrolysate (CH) was obtained from leather industry trimming waste through enzymatic hydrolysis, whereas SDS-PAGE analysis verified that the resulting hydrolysate possessed a type I structure. Hydroxyapatite, a major mineral component of bone tissue, exhibits high biocompatibility and bioactivity. With the aim of enhancing water barrier properties, CH-based films were evaluated for thickness, moisture content (MC, %), water solubility (WS, %), and water vapor permeability (WVP) following the incorporation of hydroxyapatite nanoparticles. The addition of 4% hydroxyapatite nanoparticles increased film thickness from 0.131 mm to 0.159 mm, while reducing MC and WS from 19.302% to 12.556% and from 37.016% to 21.232%, respectively, indicating improved water resistance. WVP similarly decreased from 1.649 to 1.073 × 10-11 g/Pa·h·m. These findings indicate that CH-based films containing hydroxyapatite nanoparticles can serve as environmentally friendly functional packaging materials.

Keywords: Leather, Waste, Collagen, Hydroxyapatite, Film

TREND ANALYSIS OF METEOROLOGICAL DROUGHT INDICES (SPI, ASPI AND SPEI) IN BOZCAADA

YUSUF ALPEREN KAYNAR
Çanakkale Onsekiz Mart University, Faculty Of Engineering, Civil Engineering
y.alperen.kaynar@gmail.com

Assist. Prof. Dr. FEVZİYE AYÇA SARAÇOĞLU
Çanakkale Onsekiz Mart University, Faculty Of Engineering, Civil Engineering
favarol@comu.edu.tr

Abstract
Drought is a complex climatic phenomenon that creates significant impacts on the hydrological cycle, ecosystems, and agricultural and socio-economic stability as a result of prolonged precipitation deficits. In this study, meteorological drought trends for the Bozcaada station in Çanakkale Province were analyzed for the period 1967–2023. Monthly total precipitation and average temperature data obtained from the Turkish State Meteorological Service (TSMS) were used, and potential evapotranspiration (PET) was calculated from these data. Three precipitation-based meteorological drought indices were applied: the Standardized Precipitation Index (SPI), which depends only on precipitation; the Agricultural Standardized Precipitation Index (aSPI), which incorporates effective precipitation; and the Standardized Precipitation–Evapotranspiration Index (SPEI), which accounts for potential evapotranspiration effects.The indices were computed for 1-, 3-, 6-, and 12-month time scales, and trends were evaluated using the Mann–Kendall test and Sen's slope estimator at a 5% significance level.According to the results, no statistically significant trend was detected in the SPI and aSPI indices for Bozcaada, whereas the SPEI index exhibited statistically significant negative trends across all time scales. For the 12-month time scale, the SPEI trend slope was determined as −0.00123 per month. These findings indicate that in Bozcaada's Dry-Subhumid climate, drought trends become more evident in indices that consider temperature and evapotranspiration effects. The combined use of multiple precipitation-based indices incorporating different climatic components enhances the reliability and representativeness of regional drought assessments.

Keywords: Drought Analysis, Bozcaada, Standardized Precipitation Index (spi), Agricultural Standardized Precipitation Index (aspi), Standardized Precipitation-evapotranspiration Index (spei), Trend Analysis

DETERMINATION END EVALUAITON OF RHEOLOGICAL PROPERTIES OF SOLID LUBRICANTS ON CALCIUM GREASES

Expert SEVDA ATAR
Hacettepe University, Chemistry, Potem
ssahan@petrolofisi.com.tr

Expert ALİZE PINAR
Yıldız Technical University, Cehmistry, Potem
alize.pinar@petrolofisi.com.tr

Abstract
Calcium greases have the potential to be an effective alternative to lithium greases when formulated effectively. Solid lubricants are often used to enhance the performance properties of such materials. But for what purpose? This study was conducted with molybdenum disulfide, one of the most widely used solid lubricants in industry. To demonstrate the rheological effects of molybdenum disulfide, we added solid lubricants to calcium greases formulated by our laboratory at concentrations of 0%, 0.5%, 1%, 3%, 5%, 7%, 10%, and 20%. We then evaluated and reported the rheological effects by measuring the performance effects of the solid lubricant on the calcium grease.

Keywords: Solid Lubricants, Calcium Grases, Molibdenum Disulfide, Rheological Properties

FULL TEXT PAPERS

In this area, there are full-text papers sent to the Incohis 2025 Autumn congress that meet the conditions of the congress.

LASTİKLERİN YUVARLANMA DİRENCİ KATSAYISININ (RRC) N2 KATEGORİ ELEKTRİKLİ KARGO VAN ARAÇLARDA ENERJİ TÜKETİMİNE ETKİSİ

AHMET SERDAR SERTER

Koluman Otomotiv Endüstri A.Ş., ARGE Departmanı, Mersin, Türkiye
serdar.serter@koluman.com, ORCID: 0009-0004-4320-7367

Özet

Kargo Van araçlar, tasarım itibariyle yükseklik ve genişliklerinden dolayı yüksek hava direncine sahip araçlardır. Bu çalışmada Avrupa lastik etiketine sahip bir lastiğin sınır değerlerindeki farklı yuvarlanma direnci katsayısına (RRC) sahip lastikler kullanılarak kargo van elektrikli aracın enerji tüketimleri karşılaştırılmıştır. Aynı zamanda farklı yuvarlanma direnci katsayısına (RRC) sahip lastiklerin verimliliğe etkisi gözlemlenmiştir.

Sınır değerleri lastiğin enerji etiketi baz alınarak AB 2020/740 lastiklerin yakıt verimliliği ve diğer parametreler açısından etiketlenmesi hakkında yönetmeliğine göre sınıflandırma tablosunda yer alan 6.1 N/kN yuvarlanma direnci katsayısı (RRC) ve 7.0 N/kN yuvarlanma direnci katsayısına (RRC) sahip 215/75 R17.5 ebatında lastikler VECTO (Vehicle Energy Consumption Calculation Tool) programında van elektrikli aracımızı çeşitli yol senaryolarında simülasyonu gerçekleştirilmiş ve verim değerleri alınmıştır. Analiz sonuçlarına göre 6.1 N/kN yuvarlanma direnci katsayısına (RRC) sahip lastikte enerji tüketimi 0.6588 kWh/km, Sıfır CO_2 emisyonu ile kat edilebilen menzil ise 38.3 km olduğu gözlemlenmiş olup 7.0 N/kN yuvarlanma direnci katsayısına (RRC) sahip lastikte ise enerji tüketimi 0.6724 kWh/km, sıfır CO_2 emisyonu ile kat edilebilen menzil ise 37.5 km olduğu gözlemlenmiştir.
Analiz sonuçlarına istinaden 6,1 N/kN yuvarlanma direnci katsayısına (RRC) sahip lastiğin 7,0 N/kN yuvarlanma direnci katsayısına (RRC) sahip lastikğe göre enerji tüketimi verimi %2.06 iken sıfır CO_2 emisyonu ile kat edilebilen menzil verimi ise %2.1 olarak hesaplanmıştır. Hesapladığımız sonuçlara göre yuvarlanma katsayısındaki azalma ile kargo van elektrikli aracın enerji tüketimine ve sıfır CO_2 emisyonu ile kat edilebilen menzil verimine olumlu yönde etki ettiği gözlemlenmiştir.

Anahtar Kelimeler: VECTO, RRC, yuvarlanma direnci, emisyon, enerji tüketimi, sıfır CO_2 emisyonu

THE EFFECT OF ROLLING RESISTANCE COEFFICIENT (RRC) OF TIRES ON ENERGY CONSUMPTION IN N2 CATEGORY ELECTRIC CARGO VAN VEHICLES

Abstract

Cargo van vehicles inherently have high aerodynamic drag due to their height and width. In this study, the energy consumption of an N2 category electric cargo van was compared by using tires with different rolling resistance coefficients (RRC) within the limit values specified on the European tire label. At the same time, the effect of different RRC values on vehicle efficiency was observed.

Based on the classification table in Regulation (EU) 2020/740 on the labeling of tires with respect to fuel efficiency and other parameters, simulations were performed in the VECTO (Vehicle Energy Consumption Calculation Tool) program using 215/75 R17.5 tires with rolling resistance coefficients (RRC) of 6.1 N/kN and 7.0 N/kN for various road scenarios of the electric van. According to the analysis results, the tire with an RRC of 6.1 N/kN showed an energy consumption of 0.6588 kWh/km and a zero CO_2 emission driving range of 38.3 km, while the tire with an RRC of 7.0 N/kN showed an energy consumption of 0.6724 kWh/km and a zero CO_2 emission driving range of 37.5 km.
Based on the analysis, the tire with an RRC of 6.1 N/kN provided 2.06% better energy efficiency and a 2.1% longer zero CO_2 emission range compared to the tire with an RRC of 7.0 N/kN. The results indicate that reducing the rolling resistance coefficient positively affects the energy consumption and zero CO_2 emission driving range of electric cargo vans.
Keywords: VECTO, RRC, rolling resistance, emission, energy consumption, zero CO_2 emission

1. GİRİŞ

Küresel ulaşım sektörü, enerji tüketimi ve sera gazı emisyonlarındaki payı nedeniyle sürdürülebilir kalkınma ve iklim değişikliği ile mücadele hedeflerinin merkezinde yer almaktadır. Bu bağlamda, Avrupa Birliği (AB), özellikle ağır hizmet taşıtlarından kaynaklanan karbon ayak izini azaltmaya yönelik iddialı politikalar ve bağlayıcı mevzuatlar geliştirmiştir. Bu düzenlemelerin temel taşlarından biri, yeni ağır hizmet taşıtları için CO_2 emisyon standartlarını belirleyen ve Ağır Hizmet Taşıtları için CO_2 Emisyonları ve Yakıt Tüketiminin Belirlenmesine İlişkin Yönetmelik (AB) 2017/2400'dür. Söz konusu yönetmelik, üreticilerin emisyon değerlerini hesaplamak için VECTO (Araç Enerji Tüketimi Hesaplama Aracı) yazılımını kullanmasını zorunlu kılmıştır.

Bu çalışma, teknik olarak izin verilen azami yüklü ağırlığı 6.500 kg olan ve Araçların Genel Güvenliği ve Koruyucu Sistemlerinin İşlevselliğine İlişkin Pazar Gözetimi Yönetmeliği (AB) 2018/858'in 4(1)'inci maddesinin (b)(ii) bendi uyarınca 'medium lorry' (hafif/orta yük kamyonu) kategorisinde değerlendirilen N2 sınıfı bir aracın (AB 2018/858), Ağır Vasıta Taşıtları için CO_2 Emisyonları ve Yakıt Tüketiminin Belirlenmesine İlişkin Yönetmelik (AB) 2017/2400 kapsamında VECTO (Araç Enerji Tüketimi Hesaplama Aracı) simülasyonlarına dahil edilme sürecini incelemektedir (AB 2017/2400). Araştırmanın temel amacı, söz konusu araca ait 215/75 R17.5 ebatındaki lastiklerinin, Lastiklerin Yakıt Verimliliği ve Diğer Parametrelere İlişkin Etiketleme Koşullarına Dair Tüzük (AB) 2020/740'ta tanımlanan lastik enerji verimliliği sınıflandırması ve RRC (Döngüsel Direnç Katsayısı) aralıkları dikkate alınarak, farklı RRC değerlerinin aracın toplam enerji tüketimi ve buna bağlı olarak sıfır CO_2 emisyonu ile kat edilebilen menzil üzerindeki etkisini niceliksel olarak hesaplamak ve karşılaştırmaktır. Çalışma kapsamında, lastik verimliliğindeki artışın, taşıtın genel enerji verimliliğine ve operasyonel karbon ayak izine olan katkısını ortaya koyan kapsamlı bir verimlilik analizi gerçekleştirilecektir.

2. ÇALIŞMANIN YÖNTEMİ

Bu bölüm, çalışmada kullanılan sanal araç modeli, lastik parametreleri, simülasyon yazılımı ve analiz metodolojisinin detaylarını içermektedir.

2.1. Araç Modeli ve Temel Özellikleri

Çalışmada, Avrupa Birliği düzenlemeleri kapsamında "medium lorry" olarak sınıflandırılan, tamamen elektrikli N2 kategorisi kargo van aracı temel alınmıştır. Araç modeli, sektörde yaygın kullanılan ve yüksek karoser hacmi ile karakterize edilen bir tasarımı yansıtacak şekilde oluşturulmuştur. Araca ait temel teknik özellikler Tablo 1'de özetlenmiştir.

Tablo 1: Araç Teknik Özellikleri

Elektrik Motoru Maks. Net Güç	150 kW
Batarya	141 kWh
Araç Uzunluğu	7.49 m
Araç Genişliği	2.0 m
Araç Yüksekliği	2.675 m
Aks merkezleri arasındaki uzunluk	4.325 m
Kargo Hacmi	16.3 m3
Aks konfigurasyonu	4x2 (arka aks çift lastik)
Üstyapı Kodu	BB
Aracın Yürür Vaziyetteki Kütlesi	4050 kg
Azami Yüklü Kütle	6500 kg
Lastik/Yuvarlanma Direnci Katsayısı	215/75 R17.5 – 6.1 N/kN ve 7.0 N/kN

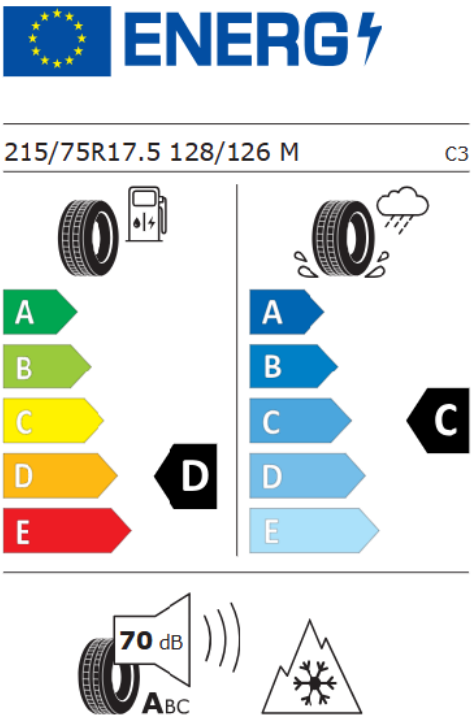
2.2. Lastik Seçimi ve Parametreler

Lastiklerin yuvarlanma direncinin (Rolling Resistance Coefficient - RRC) etkisini izole etmek amacıyla, aynı ebatta (215/75 R17.5) ancak farklı RRC değerlerine sahip iki farklı lastik seti seçilmiştir. Lastiklerin

RRC değerlerinin belirlenmesinde (AB) 2020/740 Lastik Etiketleme Tüzüğü'ndeki sınıflandırma aralıkları referans alınmıştır. İncelenen lastiklere ait parametreler Tablo 2'de verilmiştir.

Tablo 2: Lastik Etiketleme Tüzüğü (AB 2020/740)

Yakıt Verimliliği Sınıfı	C1 Lastikleri (RRC - N/kN)	C2 Lastikleri (RRC - N/kN)	C3 Lastikleri (RRC - N/kN)
A	RRC ≤ 6,5	RRC ≤ 5,5	RRC ≤ 4,0
B	6,6 ≤ RRC ≤ 7,7	5,6 ≤ RRC ≤ 6,7	4,1 ≤ RRC ≤ 5,0
C	7,8 ≤ RRC ≤ 9,0	6,8 ≤ RRC ≤ 8,0	5,1 ≤ RRC ≤ 6,0
D	9,1 ≤ RRC ≤ 10,5	8,1 ≤ RRC ≤ 9,0	6,1 ≤ RRC ≤ 7,0
E	RRC ≥ 10,6	RRC ≥ 9,1	RRC ≥ 7,1



Şekil 1: İncelenen Lastiklere Ait Parametreler (LASİD, 2020)

Lastik etiketinde yer alan bilgiler doğrultusunda, AB 2020/740 Yönetmeliği'nde belirtilen RRC tablosuna göre değer aralığımız 6,1 ≤ RRC ≤ 7,0 olarak belirlenmiştir.

2.3. Simülasyon Yazılımı ve Senaryolar

Enerji tüketimi ve menzil hesaplamaları, Avrupa Komisyonu tarafından ağır vasıta taşıtları için CO_2 emisyonlarının resmi olarak belirlenmesinde kullanılan VECTO (Vehicle Energy Consumption Calculation Tool) v5.0.3. yazılımı ile gerçekleştirilmiştir. Yazılımın doğrulanmış fiziksel temelli modelleri, bu çalışmanın güvenilirliğini sağlamaktadır.

Simülasyonlar, kentsel dağıtım ve bölgesel dağıtım gibi tipik kargo van operasyonlarını temsil eden, VECTO'nun ön tanımlı "Regional Delivery – RD" ve "Urban Delivery – UD" sürüş çevrimlerinde yapılmıştır (*VECTO, 2018).*

2.4. Veri Analizi Yöntemi

Her bir lastik seti ve sürüş çevrimi kombinasyonu için VECTO yazılımı tarafından hesaplanan enerji tüketimi (kWh/km) ve sıfır CO_2 emisyonu ile kat edilebilen menzil (km) çıktıları kaydedilmiştir. Performans karşılaştırması, aşağıdaki formüller kullanılarak yapılmıştır:

Enerji tüketimi iyileşmesi (%) = [(Enerji_Tüketimi_Yüksek_RRC - Enerji_Tüketimi_Düşük_RRC) / Enerji_Tüketimi_Yüksek_RRC] x 100

Sıfır CO_2 emisyonu ile kat edilebilen menzil iyileşmesi (%) = [(Menzil_Düşük_RRC - Menzil_Yüksek_RRC) / Menzil_Yüksek_RRC] x 100

Bu niceliksel analiz, lastik yuvarlanma direncinin N2 kategori elektrikli kargo van aracımız üzerindeki net etkisini ortaya koymayı amaçlamaktadır.

3. BULGULAR VE TARTIŞMA

3.1. BULGULAR

Araçla ilgili teknik özellikler ve değerler VECTO programının veri tabanına girildikten sonra bölgesel teslimat ve kentsel teslimat yol koşullarını değerleri ve ortalama sonuç değerleri elde edilmiştir.

İlk olarak 215/65 R22.5 ebat ve 6.1 N/kN yuvarlanma direnci katsayısına (RRC) sahip N2 kategori elektrikli kargo van aracımızı VECTO programı üzerinde simüle ederek ortalama sonuç değerleri aşağıdaki tabloda verilmiştir.

Tablo 3: RRC – 6.1 N/kN lastiğe sahip aracın ortalama sonuç değerleri

Parametre	**Değer**	**Birim**
Ortalama Taşıma Yükü	0,615	ton
Enerji Tüketimi (kWh/km)	0,6588	kWh/km
Enerji Tüketimi (kWh/t-km)	1,070	kWh/t-km
Enerji Tüketimi (kWh/m³-km)	0,04041	kWh/m³-km
Enerji Tüketimi (MJ/km)	2,372	MJ/km
Enerji Tüketimi (MJ/t-km)	3,854	MJ/t-km
Enerji Tüketimi (MJ/m³-km)	0,1455	MJ/m³-km
Gerçek Şarj Boşalma Menzili	38,3	km
Eşdeğer Tam Elektrikli Menzil	38,3	km
Sıfır CO_2 Emisyon Menzili	38,3	km

N2 kategori elektrikli kargo van aracımızda 215/75 R17.5 ebat ve 6.0 N/kN yuvarlanma direnci katsayısına (RRC) sahip lastik kullanıldığında, Şekil 1'de gösterildiği gibi enerji tüketimi 0.6588 kWh/km, Sıfır CO_2 emisyonu ile kat edilebilen menzil ise 38.3 km dir.

215/65 R22.5 ebat ve 7.0 N/kN yuvarlanma direnci katsayısına (RRC) sahip N2 kategori elektrikli kargo van aracımızı VECTO programı üzerinde simüle ederek ortalama sonuç değerleri aşağıdaki tabloda verilmiştir.

Tablo 4: RRC – 7.0 N/kN lastiğe sahip aracın ortalama sonuç değerleri

Parametre	**Değer**	**Birim**
Ortalama Taşıma Yükü	0,615	ton

Enerji Tüketimi (kWh/km)	0,6724	kWh/km
Enerji Tüketimi (kWh/t-km)	1,093	kWh/t-km
Enerji Tüketimi (kWh/m³-km)	0,04125	kWh/m³-km
Enerji Tüketimi (MJ/km)	2,421	MJ/km
Enerji Tüketimi (MJ/t-km)	3,934	MJ/t-km
Enerji Tüketimi (MJ/m³-km)	0,1485	MJ/m³-km
Gerçek Şarj Boşalma Menzili	37,5	km
Eşdeğer Tam Elektrikli Menzil	37,5	km
Sıfır CO_2 Emisyon Menzili	37,5	km

N2 kategori elektrikli kargo van aracımızda 215/75 R17.5 ebat ve 7.0 N/kN yuvarlanma direnci katsayısına (RRC) sahip lastik kullanıldığında, Şekil 1'de gösterildiği gibi enerji tüketimi 0.6724 kWh/km, Sıfır CO_2 emisyonu ile kat edilebilen menzil ise 37.3 km dir.

3.2 TARTIŞMA

Simülasyon sonuçları incelendiğinde, yuvarlanma direnci katsayısı (RRC) arttıkça aracın enerji tüketiminin yükseldiği ve buna bağlı olarak sıfır CO_2 emisyon menzilinin azaldığı görülmektedir. RRC değeri 6,1 N/kN olan lastik kullanıldığında enerji tüketimi 0,6588 kWh/km seviyesinde iken, RRC değeri 7,0 N/kN olan lastikte bu değer 0,6724 kWh/km'ye çıkmıştır. Bu artış küçük görünse de menzil üzerinde doğrudan etki yaratmış ve aracın sıfır emisyonla kat edebildiği mesafe 38,3 km'den 37,5 km'ye düşmüştür. Bu durum, lastiklerin yuvarlanma direnci katsayısının özellikle elektrikli araçlarda menzil performansı açısından kritik bir parametre olduğunu göstermektedir.

4. SONUÇ

Elde edilen bulgular, düşük yuvarlanma direncine (RRC) sahip lastiklerin N2 kategori elektrikli kargo vanlarda enerji verimliliğini artırarak sıfır CO_2 emisyon menzilini uzattığını göstermektedir. RRC'nin 6,1 N/kN seviyesinde tutulması, enerji tüketiminde %2,06 oranında tasarruf sağlarken, sıfır CO_2 emisyonu ile %2,1 daha uzun menzil kazandırmaktadır. Bu nedenle, filo ve operasyonel verimlilik açısından düşük RRC değerine sahip lastiklerin tercih edilmesi, hem enerji maliyetlerinin azaltılmasına hem de sürdürülebilirlik hedeflerinin desteklenmesine katkı sağlamaktadır.

KAYNAKÇA

AB 2017/2400. 18 Aralık 2017 tarihli, ağır hizmet araçlarının CO_2 emisyonlarının ve yakıt tüketiminin belirlenmesine ilişkin (AB) 2017/2400 sayılı Yönetmelik.

AB 2018/858. 30 Mayıs 2018 tarihli, motorlu araçların onayı ve piyasa gözetimine ilişkin (AB) 2018/858 sayılı Yönetmelik.

AB 2020/740. 25 Mayıs 2020 tarihli, lastiklerin yakıt verimliliği ve diğer parametreler bakımından etiketlenmesine ilişkin (AB) 2020/740 sayılı Yönetmelik.

VECTO,2018. Araç Enerji Tüketimi Hesaplama Aracı. https://climate.ec.europa.eu/eu-action/transport-decarbonisation/road-transport/vehicle-energy-consumption-calculation-tool-vecto_en

LASİD, 2020. https://www.lasid.com.tr/lastik/lastik-hakkinda-her-sey/lastigin-teknik-ozellikleri/lastigin-etiketlemesi/

FİLM KALİTESİ TAHMİNİ: METİN, GÖRSEL VE TABLO VERİLERİNİ KULLANARAK OPTİMİZE EDİLMİŞ ÇOK MODLU YIĞINLAMA YAKLAŞIMI

TAYFUN DURMUŞ
Kocaeli Üniversitesi, Fen Bilimleri Enstitüsü, Yazılım Mühendisliği, Kocaeli, Türkiye
tayfundurmus23@gmail.com, ORCID: 0009-0003-1200-5220

Doç. Dr. HAKAN GÜNDÜZ
Kocaeli Üniversitesi, Fen Bilimleri Enstitüsü, Yazılım Mühendisliği, Kocaeli, Türkiye
hakan.gunduz@kocaeli.edu.tr, ORCID: 0000-0003-2152-5490

Özet

Bu çalışmanın amacı, film kalitesini (kritik bir regresyon problemi) tahmin etmek için metinsel, görsel ve tablosal özellikleri birleştirerek performansı (R^2) değerlendiren çok modlu (multimodal) bir makine öğrenimi modeli geliştirmektir. Çeşitli özellik çıkarma motorları (CLIP, mpnet, vb.), önişleme stratejileri ve model mimarileri analiz edilmiştir. TMDB'den alınan 9.915 filmlik bir veri seti kullanılmıştır. Oy sayısına göre filtrelemenin etkisi araştırılmıştır. Özellik çıkarımı için, metinsel verilerde all-mpnet-base-v2, görsel verilerde clip-ViT-B-32 kullanılmış ve beş temel tablosal özellik (örn. popülerlik, oy_sayısı) kullanılmıştır. Özellik seçiminin (SelectKBest) ve ölçeklendirmenin (StandardScaler) performans üzerindeki etkisi de analiz edilmiştir. Nihai model, filtrelenmiş çok modlu veri seti üzerinde RandomizedSearchCV ile optimize edilmiş LightGBM, XGBoost ve CatBoost modellerini birleştiren bir StackingRegressor'a (meta-model: RidgeCV) dayanmaktadır. Filtrelenmiş veri setinde (≥ 400 oy), parça analizi (ablation study) dikkate değer bir görsel sinyal (CLIP $R^2 \approx 0{,}21$) ortaya koyarken, tüm özellikleri birleştiren optimize edilmiş nihai yığınlama (stacking) modeli, test $R^2 = 0{,}6027$ sonucunu elde etmiştir. Bu çalışma, tablosal meta verilerin baskın sinyal olduğunu doğrulamaktadır. Ancak, güçlü kodlayıcılarla (all-mpnet-base-v2, clip-ViT-B-32) işlenen metinsel ve poster verileri, tek başına tablosal verilerde bulunmayan benzersiz bilgiler sunarak model performansını artırmıştır. En yüksek başarıya (1) veri filtreleme (≥ 400 oy), (2) etkili kodlayıcılar (clip-ViT-B-32) ve (3) optimize edilmiş model yığınlamasının sinerjisi ile ulaşılmıştır. Bu metodoloji, film kalitesindeki varyansın %60.2'sini başarıyla açıklamaktadır.

Anahtar Kelimeler: Film Kalitesi Tahmini, Çok Modlu Regresyon, Yığınlama, CLIP, S-BERT, R^2

FILM QUALITY PREDICTION: AN OPTIMIZED MULTIMODAL STACKING APPROACH USING TEXTUAL, VISUAL AND TABULAR DATA

Abstract

This study's objective is to develop a multimodal machine learning model for predicting film quality (a critical regression problem) by integrating textual, visual, and tabular features to evaluate performance (R^2). Various feature extraction engines (CLIP, mpnet, etc.), preprocessing strategies, and model architectures were analyzed. A 9,915 film dataset from TMDB was used. The effect of filtering by vote count was investigated. For feature extraction, textual data used all-mpnet-base-v2, visual data used clip-ViT-B-32, and five key tabular features (e.g., popularity, vote_count) were employed. The impact of feature selection (SelectKBest) and scaling (StandardScaler) on performance was also analyzed. The final model is based on a StackingRegressor (meta-model: RidgeCV) that combines LightGBM, XGBoost, and CatBoost models, each optimized via RandomizedSearchCV over the filtered multimodal dataset. On the filtered dataset (≥ 400 votes), ablation analysis revealed a notable visual signal (CLIP $R^2 \approx 0.21$), while the final optimized stacking model combining all features achieved a test $R^2 = 0.6027$. This study confirms tabular metadata is the dominant signal. However, textual and poster data processed with powerful encoders (all-mpnet-base-v2, clip-ViT-B-32) contributed unique information not in tabular data alone, enhancing model performance. The highest success was achieved through the

synergy of (1) data filtering (≥ 400 votes), (2) effective encoders (clip-ViT-B-32), and (3) optimized model stacking. This methodology successfully explains 60.2% of the variance in film quality.

Keywords: Film Quality Prediction, Multimodal Regression, Stacking, CLIP, S-BERT, R^2

1. GİRİŞ

Film endüstrisi, yüksek yatırım maliyetleri ve belirsiz getiri oranları ile karakterize edilen, ekonomik açıdan yüksek riskli bir sektördür. Bu nedenle, bir filmin kalitesini veya ticari başarısını tahmin edebilen modeller geliştirmek, sektör paydaşlarının karar alma süreçlerini optimize etmesi açısından kritik bir öneme sahiptir.

Literatürdeki mevcut çalışmaların bir kısmı, film başarısını "gişe hasılatı" tahmini üzerinden ele almaktadır. Bu çalışmalarda (Ni vd., 2022 ; Zhang vd., 2024), toplam gişeyi tahmin etmek için "ilk hafta gişesi" veya "arama indeksi" gibi veriler kullanılarak yüksek başarı skorlarına (Ni vd., 2022 için R^2=0.89) ulaşıldığı görülmektedir.

Literatürdeki diğer bir güncel eğilim ise, film metinlerini (Dhawan vd., 2025 ; Pandey vd., 2024) veya çok modlu verileri (Yoon vd., t.y.) bir Sınıflandırma (Classification) problemi olarak ele almaktır. Bu çalışmalar, metinleri 'Pozitif/Negatif' olarak etiketler veya filmleri 'Başarılı/Başarısız' olarak sınıflandırır. Bu yaklaşımlar değerli olmakla birlikte, bir filmin kalitesindeki nüansları (örneğin "6.5" ile "7.5" puan arasındaki farkı) yakalamada yetersiz kalmaktadır.

Bizim çalışmamız ise, bu iki yaklaşımdan farklı olarak, daha zorlu bir problem olan Regresyon (Regression) problemine, yani 0-10 arası kalite puanının doğrudan tahmin edilmesine odaklanmaktadır. Literatürdeki (Yang vd., 2019) benzer "çok modlu puan tahmini" çalışmalarını referans alan bu makale, film başarısını tahmin etmede yaygın olarak kullanılan 'tek-modlu' (uni-modal), yani sadece tablosal verilere (popülerlik ve oy sayısı gibi) dayalı yaklaşımın sınırlamalarını ele almaktadır.

Bu çalışmanın temel katkısı, filmin "ruhunu" oluşturan metinsel (özet) ve görsel (poster) verilerin, zaten güçlü olan tablosal verilere eklenmesinin (yani "Çok Modlu" bir yaklaşımın), film kalitesi tahmin skorunu (R^2) anlamlı ölçüde artırıp artırmadığını kanıtlamaktır.

Bu tezi test etmek için, metinsel özetlerden S-BERT ile, poster görsellerinden ise CLIP ile anlamsal özellikler çıkarılmış ve bu özellikler tablosal verilerle birleştirilmiştir. Bu birleşik veri seti (1312 özellik), RandomizedSearchCV ile optimize edilmiş ve LightGBM, XGBoost, CatBoost gibi güçlü modelleri içeren bir Yığınlama (Stacking) mimarisiyle modellenmiştir.

Makalenin geri kalanı şu şekilde yapılandırılmıştır: Bölüm 2'de kullanılan veri seti, özellik çıkarımı ve Yığınlama metodolojisi detaylandırılmaktadır. Bölüm 3'te Parça Analizi (Ablation Study) bulguları ve nihai model sonuçları (R^2=0.6027) sunulmakta ve bu sonuçlar literatür bağlamında tartışılmaktadır. Son olarak genel sonuçlar ve gelecek çalışma önerileri özetlenmektedir.

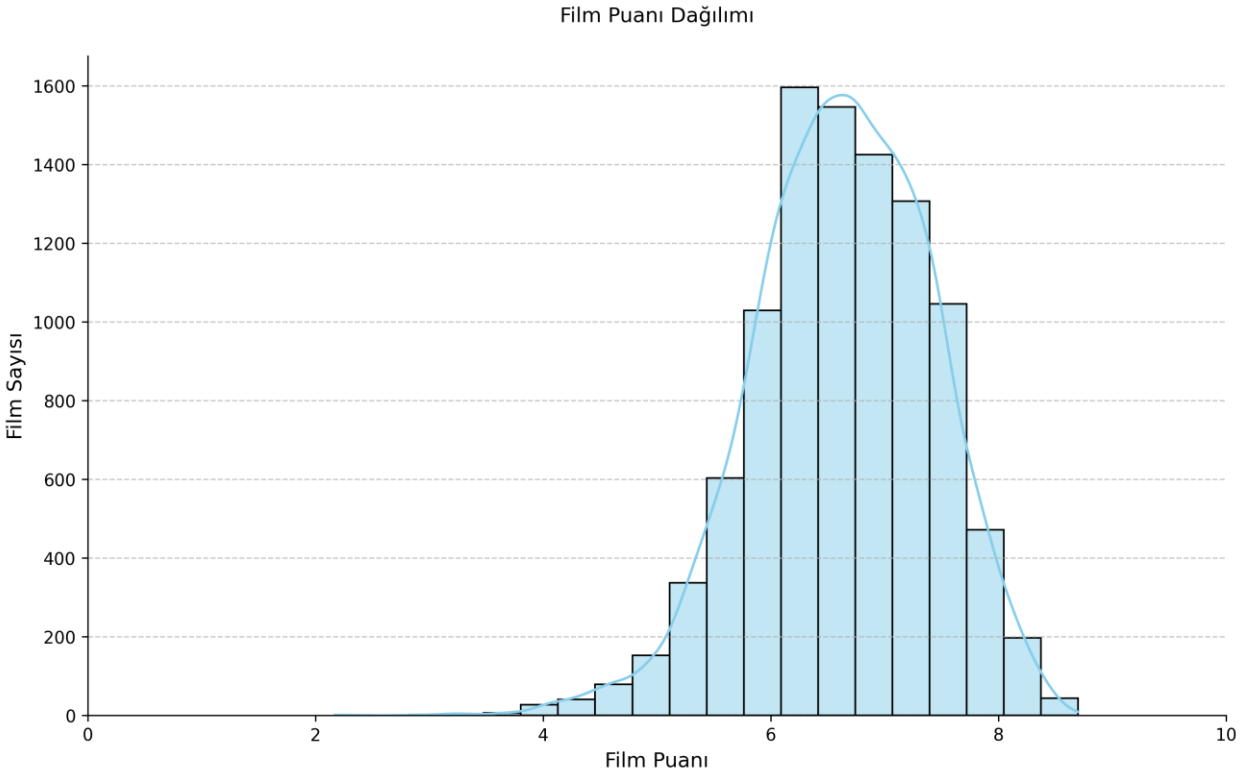
2. ÇALIŞMANIN YÖNTEMİ

Bu bölümde, çok modlu film kalitesi tahmin modeli geliştirmek için izlenen metodoloji detaylandırılmaktadır. Sırasıyla; kullanılan veri seti, bu verilerden özellik çıkarma yöntemleri, en iyi özellikleri bulmak için yapılan deneysel tasarım, değerlendirme metrikleri, bu özellikleri modellemek için kullanılan Yığınlama (Stacking) mimarisi ve son olarak modelin açıklanabilirliği için kullanılan yöntem açıklanmaktadır.

2.1. Veri Seti ve Hedef Değişken

Çalışmada kullanılan veri seti, film endüstrisi hakkında kapsamlı veriler sunan The Movie Database (TMDB) platformundan (Arun4545, t.y.) alınmış 9.915 filmlik ham bir veri setidir. Bizim modelimizin hedef değişkeni (Y), bir Regresyon problemi olan, filmlerin 0-10 arası 'vote_average' (ortalama puan) değeridir.

Şekil 1'de görüldüğü gibi, bu puanların dağılımı normal bir dağılım göstermemekte, 6 ile 8 puan aralığında yoğun bir şekilde yığılmış durumdadır. Bu yığılma, modelin özellikle orta puanlı filmleri, yüksek puanlı filmlerden ayırt etmesinin zor olacağını, yani problemin zorluğunu ortaya koymaktadır.



Şekil 1: Film Puanı Dağılımı

2.2. Çok Modlu Özellik Mühendisliği (Feature Engineering)

Modelimizin ham veriyi işleyebilmesi için, "Giriş" bölümünde bahsedilen üç temel veri türüne dayalı bir özellik mühendisliği süreci uygulanmıştır. Metinsel Veri (Textual Data) için, filmin 'overview' (özet) metinleri, sentence-transformers kütüphanesinde bulunan S-BERT (all-mpnet-base-v2) modeli kullanılarak anlamsal vektörlere dönüştürülmüştür. Bu işlem sonucunda her film için 768 boyutlu bir metin vektörü elde edilmiştir. Görsel Veri (Visual Data) için, filmlerin hem 'poster' resimleri hem de 'backdrop' (arka plan) resimleri, sentence-transformers kütüphanesi aracılığıyla CLIP (ViT-B-32) modeline verilmiştir. Bu işlem, her iki görsel türü için de ayrı ayrı 512 boyutlu vektörler üretmiştir. Hangi görsel verinin daha etkili olduğunun tespiti için Bölüm 3.1.1'de Parça Analizi yapılmış ve 'poster' verisinin daha iyi sonuç verdiği görüldüğü için nihai modelde 'poster' verisi kullanılmıştır. Son olarak, Tablosal Veri (Tabular Data) için popularity (popülerlik), vote_count (oy sayısı), release_date (yayınlanma tarihi), original_language (dil) ve genre_ids (tür) olmak üzere 5 temel özellik kullanılmıştır. Bu kategorik ve sayısal veriler, standart önişleme (One-Hot encoding) ile 32 boyutlu bir vektöre dönüştürülmüştür. Sonuç olarak, bu üç modun birleştirilmesiyle (768 + 512 + 32), her film için toplam 1312 özellikli birleşik bir çok modlu (multimodal) veri seti oluşturulmuştur.

2.3. Deneysel Tasarım ve Optimizasyon

Modelin performansını değerlendirmek için veri seti, %80 Eğitim (Train) ve %20 Test (Test) olarak bölünmüştür. En iyi skoru bulmak ve en anlamlı özellikleri belirlemek için 3 adımlı bir optimizasyon yolu izlenmiştir. İlk olarak, 'az oylu' filmlerin gürültü etkisini araştırmak için Veri Filtreleme uygulanmıştır. Bu kapsamda, 400 oydan az filmler veri setinden çıkarılmış; bu işlemin, skoru R^2 = 0.54'ten 0.57'ye çıkardığı tespit edilmiş ve final modelde 8.223 filmlik bu temizlenmiş veri seti kullanılmıştır. İkinci olarak, StandardScaler ile Veri Ölçeklendirme test edilmiş; ancak, ağaç tabanlı modeller (LGBM, XGBoost) kullanıldığı için skora anlamlı bir katkısı olmadığı görülmüştür. Üçüncü olarak, SelectKBest (f_regression ve mutual_info_regression) yöntemleriyle Özellik Seçimi test edilmiştir (9915 veri üzerinde). Tablo 1'de görüldüğü gibi, sonuçlar arasında (örn: 0.545 vs 0.542) anlamlı bir fark yaratmadığı için tam 1312 özellik ile devam edilmiştir.

Tablo 1: Özellik Seçimi (9915 Filmlik Veri Seti)

Metot	K değeri (Özellik Sayısı)	Model	R^2	MAE	RMSE
mutual_info_regression	1300	LightGBM	0.5451	0.3922	0.5233
f_regression	700	LightGBM	0.5426	0.3974	0.5248
temel model/baseline	1312	LightGBM	0.5425	0.3979	0.5248

2.4. Değerlendirme Metrikleri

Bu regresyon çalışmasında, modellerin tahmin performansını değerlendirmek için literatürde (Ni vd., 2022) yaygın olarak kullanılan üç temel metrik kullanılmıştır: R^2 (Belirlilik Katsayısı), MAE (Ortalama Mutlak Hata) ve RMSE (Kök Ortalama Kare Hata).

R^2 (Belirlilik Katsayısı), modelin hedef değişkendeki (puan) varyansın yüzde kaçını açıkladığını gösterir (1.0 mükemmel skordur).

$$R^2 = 1 - \frac{\sum_{i=1}^{n}(y_i - \hat{y}_i)^2}{\sum_{i=1}^{n}(y_i - \overline{y})^2}$$

MAE , tahminlerin gerçek değerlerden ne kadar saptığının ortalamasını gösterir ve aykırı değerlere karşı daha dayanıklıdır (0.0 mükemmel skordur).

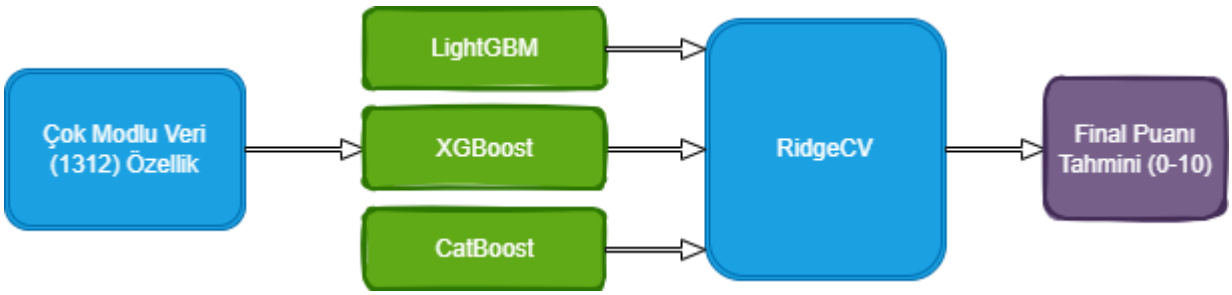
$$MAE = \frac{1}{n}\sum_{i=1}^{n}|(y_i - \hat{y}_i)|$$

RMSE , tahmin hatalarının karekökü̈dür ve özellikle büyük hataları daha fazla cezalandırır (0.0 mükemmel skordur).

$$RMSE = \sqrt{\frac{1}{n}\sum_{i=1}^{n}(y_i - \hat{y}_i)^2}$$

2.5. Final Model Mimarisi

Bu çalışmada, 1312 özellikli veri setini modellemek için, Şekil 2'de görülen 'Yığınlama' (Stacking) mimarisi tercih edilmiştir. Bu mimari, literatürde de (Ni vd., 2022) gişe tahmini gibi karmaşık regresyon problemlerinde başarısını kanıtlamıştır. Mimari şu şekilde çalışmaktadır: 'Birleşik Veri (1312 Özellik)' ilk olarak 3 güçlü temel modele (LightGBM, XGBoost, CatBoost) beslenmiştir. Bu 3 temel model, en iyi hiperparametreleri bulmak için RandomizedSearchCV kullanılarak optimize edilmiştir. İkinci aşamada, bu 3 optimize edilmiş modelin yaptığı tahminler, 'Meta-Model' olan RidgeCV'ye girdi olarak verilmiştir. Son olarak, RidgeCV bu 3 modelin tahminlerine (hangisine daha çok güveneceğine dair) nasıl ağırlık vereceğini öğrenmiş ve bu sayede Final Puan Tahminini üretmiştir.



Şekil 2: Final Model Mimarisi

2.6. Açıklanabilirlik Yöntemi (XAI)

Bu çalışmada kullanılan Yığınlama (Stacking) mimarisi 'kara kutu' (black-box) olma eğilimindedir. Modelin kararlarını yorumlamak ve "Çok Modlu" tezi kanıtlamak için SHAP (SHapley Additive exPlanations) yöntemi kullanılmıştır. Ancak, Yığınlama modelinin kendisine SHAP uygulamak, 1312 özelliğin değil, sadece 'işçi' modellerin tahminlerinin önemini göstereceği için anlamsızdır. Bu nedenle analiz, 1312 özelliğin tamamına bakan 'işçi' modellerden biri olan LightGBM üzerinde yapılmıştır. Bu yaklaşım, literatürün (Dhawan vd., 2025) 'açıklanabilirlik' (XAI) ihtiyacı vurgusunu da karşılamaktadır.

3. SONUÇ

Bu bölümde, öncelikle Bölüm 2'de açıklanan metodoloji kullanılarak elde edilen deneysel bulgular sunulmakta ve ardından bu bulguların literatürdeki diğer çalışmalar bağlamında önemi tartışılmaktadır.

3.1. Bulgular

3.1.1. Parça Analizi Sonuçları

Bu çalışmanın temel tezini (Çok Modlu > Tek Modlu) test etmek için, Bölüm 2.3'te belirlenen temizlenmiş (≥ 400 oy) veri seti üzerinde bir "Parça Analizi" (Ablation Study) yürütülmüştür. Bu analizde, 3 ana veri modunun (Metin , Görsel , Tablo) ve bunların çeşitli kombinasyonlarının R^2, MAE ve RMSE metrikleri üzerindeki etkisi, optimize edilmemiş bir LightGBM modeli kullanılarak ölçülmüştür. Sonuçlar Tablo 2'de özetlenmiştir.

Tablo 2: Parça Analizi (Ablation Study) Metrik Sonuçları

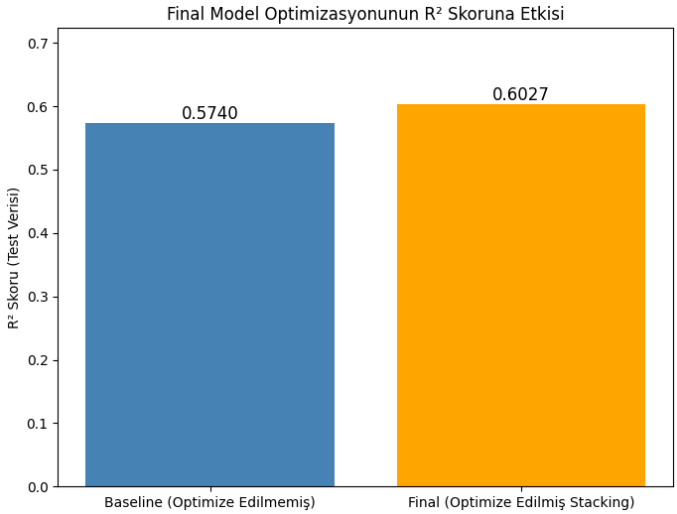
Kombinasyon	R^2	MAE	RMSE
text + tabular + poster	0.5740	0.3865	0.5067
text+tabular+poster+backdrop	0.5723	0.3884	0.5078
tabular	0.5602	0.3896	0.5149
text + tabular	0.5555	0.3922	0.5176
tabular + poster	0.5540	0.3940	0.5185
tabular + backdrop	0.5528	0.3941	0.5192
text + backdrop	0.2628	0.5141	0.6666
text + poster	0.2508	0.5224	0.6720
poster	0.2106	0.5410	0.6898
backdrop	0.2000	0.5361	0.6945
text	0.1182	0.5697	0.7291

Elde edilen bulgular çalışmamızın net bir şekilde desteklemektedir. Beklendiği gibi, oy sayısı ve popülerlik gibi güçlü özellikleri içeren Tablo verisi, R^2=0.5602 ile tek başına en güçlü sinyaldir. Ayrıca, Metin (S-BERT) (R^2=0.1182) ve Poster (CLIP) (R^2=0.2106) tek başlarına zayıf kalsalar da, modele net pozitif katkı sağladıkları doğrulanmıştır.

En Önemli Bulgumuz: "Çok Modlu" (text + tabular + poster) yaklaşım, 'Tek Modlu' (tabular) yaklaşıma göre sadece R^2 skorunu (0.5602'den 0.5740'a) yükseltmekle kalmamış, aynı zamanda ortalama tahmin hatasını (MAE) 0.3896'dan 0.3865'e düşürmüştür. Bu durum, "Çok Modlu" yaklaşımımızın, zaten güçlü olan verilere rağmen skoru daha da iyileştirdiğini kanıtlamaktadır. Ayrıca, 'backdrop' (arka plan) verisinin dahil edildiği 'TÜMÜ' (R^2=0.5723) kombinasyonunun, 'poster' içeren kombinasyondan (R^2=0.5740) daha düşük skor vermesi, final modelimizde neden 'poster' verisinin tercih edildiğini de açıklamaktadır.

3.1.2. Final Model ve Açıklanabilirlik (XAI) Bulguları

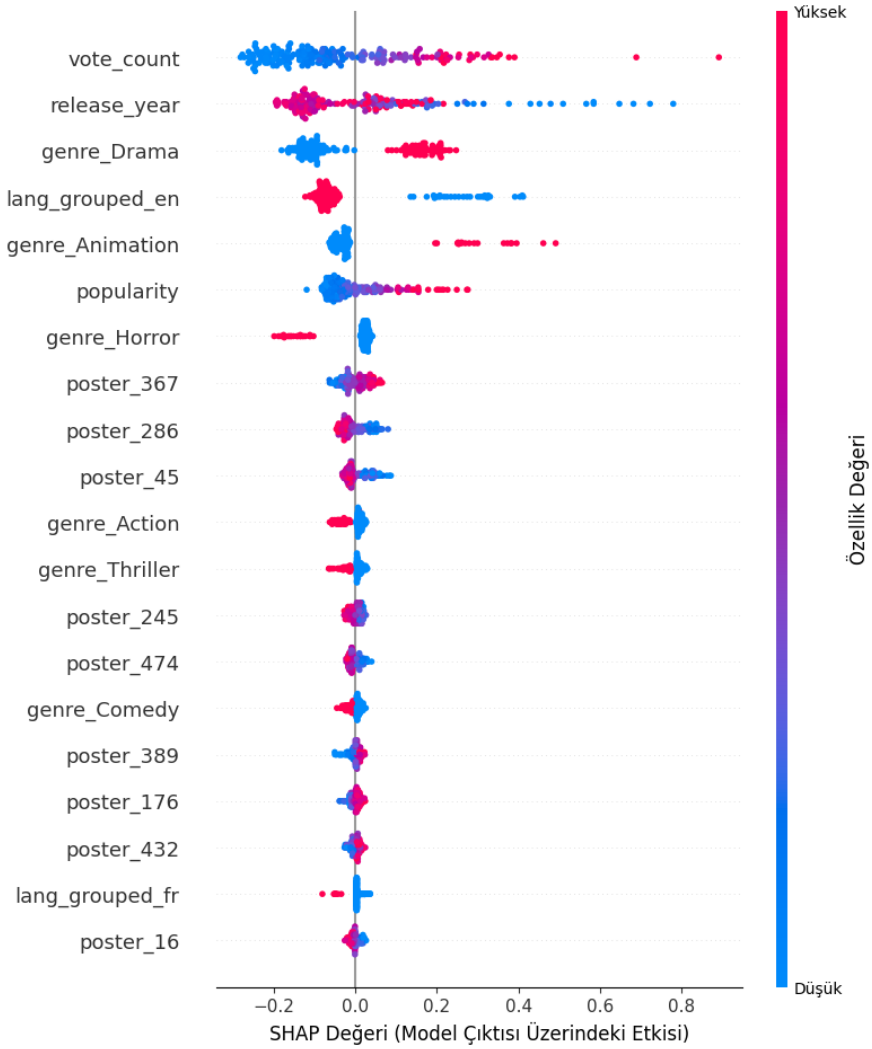
Çok Modlu" (text + tabular + poster) yaklaşımın en iyisi olduğuna karar verdikten sonra, bu 1312 özellik Bölüm 2.5'te açıklanan optimize edilmiş Yığınlama (Stacking) mimarisine beslenmiştir. Şekil 3, bu optimizasyonun (Stacking + RandomizedSearchCV) skora etkisini göstermektedir.



Şekil 3: Optimizasyonun R^2 Skoruna Etkisi

Şekil 3 incelendiğinde, Yığınlama (Stacking) ve optimizasyonun, R^2 skorunu 0.5740'dan R^2=0.6027'ye yükselttiği görülmektedir. Daha da önemlisi, bu optimizasyon, modelin ortalama tahmin hatasını MAE = 0.3727 seviyesine ve RMSE = 0.4893 seviyesine düşürmüştür. Bu, modelimizin artık filmleri 0-10'luk puan skalasında ortalama 0.37 puan hatayla tahmin edebildiğini göstermektedir.

Modelin bu kararı nasıl verdiğini anlamak için, Bölüm 2.6'da belirtildiği gibi, LightGBM modeli üzerinde SHAP analizi yürütülmüştür. Şekil 4'teki SHAP özet grafiği, modelin tahmin üzerindeki en etkili 20 özelliği göstermektedir.



Şekil 4: SHAP Özellik Önem Sıralaması (Top 20)

SHAP grafiği (Şekil 4), beklendiği gibi, vote_count ve popularity gibi tablo özelliklerinin model kararlarında en baskın özellikler olduğunu doğrulamaktadır. Ancak, poster_... (Görsel) özelliklerinin de ilk 20'de yer alması, modelin karar verirken filmin "ruhuna" (poster) aktif olarak baktığını göstermektedir. sbert_... (Metin) özelliklerinin ilk 20'ye girememiş olması, bu spesifik modelde metin katkısının diğer iki moda göre daha düşük kaldığını göstermektedir.

3.2. Tartışma

Bu çalışmada elde edilen nihai R^2=0.6027 skoru, literatürdeki diğer çalışmalarla kıyaslanırken dikkatli bir metodolojik ayrım yapılmalıdır.

Literatürdeki (Ni vd., 2022 ; Zhang vd., 2024) bazı çalışmaların 'gişe hasılatı' tahmininde yüksek başarı skorlarına (Ni vd., 2022 için R^2=0.89; Zhang vd., 2024 için %84 doğruluk) ulaştığı görülmektedir. Ancak bu metodolojiler incelendiğinde, 'toplam gişeyi' tahmin etmek için 'ilk hafta gişesi' veya 'gösterim sonrası arama indeksi' gibi verileri kullandıkları görülmektedir.

Bizim çalışmamız ise, problem tanımı açısından bu çalışmalardan farklılaşarak, 'kalite puanı' gibi daha zorlu ve öznel bir hedefi tahmin etmektedir. Bizim çalışmamızla daha doğrudan karşılaştırılabilir olan, "çok modlu" (poster+özet+tablo) verilerle "puan regresyonu" yapan çalışmalarda (Yang vd., 2019 ; Maillette de Buy Wenniger vd., 2023), R^2 skorlarının 0.425 ile 0.454 aralığında olduğu görülmektedir.

Bu bağlamda, bizim ulaştığımız R^2 = 0.6027 skoru ve ortalama 0.3727 puanlık (MAE) tahmin hatası, 'insan beğenisi' gibi öznel bir konudaki puan varyansının %60'ından fazlasını başarıyla açıkladığını

göstermekte ve benzer zorluktaki çalışmalara kıyasla anlamlı ve güçlü bir başarı olarak değerlendirilmektedir.

3.3. Sınırlılıklar ve Gelecek Çalışmalar

Bu çalışmanın temel tezi (Çok Modlu > Tek Modlu) Tablo 2'deki R^2, MAE ve RMSE değerleri ile kanıtlanmış olsa da, Şekil 4'teki SHAP analizi, sbert_... (metin) özelliklerinin model tarafından yeterince kullanılmadığını göstermiş, bu da bir sınırlılık olarak not edilmiştir. Bu durum, modelimizin metindeki sinyali görsel (CLIP) veya tablo verilerine kıyasla daha az verimli işlediğini göstermektedir. Bununla birlikte, Valera & Mehta (2024) tarafından yapılan benzer bir çalışmada, film incelemelerinden DistilBERT ile çıkarılan duygu skorlarının, regresyon modellerindeki tahmin hatasını (MSE) önemli ölçüde azalttığı kanıtlanmıştır.

Gelecekteki çalışmalarda, bu sınırlılığı aşmak için metin verisinden daha etkili duygu odaklı özelliklerin (Valera & Mehta, 2024) çıkarılması araştırılmalıdır. Ayrıca, modele filmlerin fragmanları (işitsel veri), yönetmen/oyuncu bilgileri veya senaryo metinleri gibi daha fazla mod eklenebilir ve özellik çıkarımı için S-BERT ve CLIP yerine daha büyük dil/görsel modeller (Örn: GPT-4o, ViT-L) denenebilir.

KAYNAKÇA

Arun4545. (t.y.). TMDB 10000 movies dataset [Data set]. Kaggle. Alınan tarih: 1 Nisan 2025, https://www.kaggle.com/datasets/arun4545/tmdb-10000-movies-dataset/data

Dhawan, S., Singh, K., & Yadav, M. (2025). Hybrid deep learning recommendation system for accurate movie and product review predictions. Scalable Computing: Practice and Experience, 26(4), 1902-1918

Maillette de Buy Wenniger, G., van Dongen, T., & Schomaker, L. (2023). MultiSChuBERT: Effective Multimodal Fusion for Scholarly Document Quality Prediction. arXiv. https://doi.org/10.48550/arXiv.2308.07971

Ni, Y., Dong, F., Zou, M., & Li, W. (2022). Movie box office prediction based on multi-model ensembles. Information, 13(6), 299. https://doi.org/10.3390/info13060299

Pandey, A., Yadav, R., Pathak, A., Shivani, N., Garg, B., & Pandey, A. (2024). Sentiment analysis of IMDB movie reviews. 2024 First International Conference on Software, Systems and Information Technology (SSITCON), 1-6. https://doi.org/10.1109/SSITCON62437.2024.10796578

Valera, M., & Mehta, R. (2024). Advanced Deep Learning Models for Improving Movie Rating Predictions: A Benchmarking Study. BenchCouncil Transactions on Benchmarks, Standards and Evaluations, 4, Article 100200. https://doi.org/10.1016/j.tbench.2025.100200

Yang, Y., Ma, R., & Cho, M. H. (2019). Predicting movie ratings with multimodal data. Stanford University CS229 Project. https://cs229.stanford.edu/proj2019aut/data/assignment_308832_raw/26260680.pdf

Yoon, S., Park, K., Kim, J., & Park, H. (t.y.). Multi-modal movie box office prediction using poster, review along with tabular data. CS470 Project. https://github.com/victory-jooyon/MM-movie-box-office-prediction

Zhang, Z., Meng, Y., & Xiao, D. (2024). Prediction techniques of movie box office using neural networks and emotional mining. Scientific Reports, 14, 21209. https://doi.org/10.1038/s41598-024-72340-z

GÜÇ ELEKTRONİĞİ DEVRELERİNDE DİRENÇ TOLERANSLARININ SİSTEM GÜVENİLİRLİĞİ ÜZERİNDEKİ ETKİSİNİN İNCELENMESİ

MURAT DEMİR
İzmir Bakırçay University, Department of Electrical and Electronics Engineering,
murat.demir@bakircay.edu.tr, ORCID: 0000-0003-4407-9673

Özet

Bu çalışma, güç elektroniği devrelerinde direnç toleranslarının sistem güvenilirliği üzerindeki etkisini nicel olarak incelemektedir. Dirençler çoğu zaman kritik olmayan pasif bileşenler olarak değerlendirilse de, üretim toleranslarındaki değişimler devre çalışma noktalarını dolaylı yoldan etkileyerek toplam sistem hata oranında anlamlı değişimlere neden olabilir. Bu bağlamda MIL-HDBK-217F standartlarına dayalı parça stres modeli kullanılarak yalnızca direnç bileşenlerine ait üç farklı tolerans senaryosu—minimum (±1 %), nominal (tolerans ihmal) ve maksimum (±10 %)—karşılaştırılmıştır.

Yapılan hesaplamalarda minimum tolerans senaryosunda sistemin hata oranı 3.3685 FPMH, tahmini ömür değeri 296 868 saat olarak elde edilmiştir. Maksimum tolerans senaryosunda ise hata oranı 3.5618 FPMH'ye yükselmiş, ömür değeri 280 757 saat'e düşmüştür. Nominal durumda hata oranı 3.4646 FPMH, tahmini ömür değeri ise 288 634 saat olarak hesaplanmıştır. Minimum ve maksimum tolerans senaryoları arasında %5,74 oranında hata oranı farkı ve 16 111 saatlik ömür farkı tespit edilmiştir.

Bu sonuçlar, yalnızca direnç toleransındaki değişimlerin dahi sistemin güvenilirlik göstergelerinde ölçülebilir bir etki yarattığını göstermektedir. Her ne kadar direnç bileşenleri sistemin en büyük hata kaynağı olmasa da, yüksek üretim hacmine ve uzun çalışma sürelerine sahip LED sürücü devreleri gibi uygulamalarda bu farklar toplam sistem güvenilirliği üzerinde ekonomik ve teknik açıdan anlamlı hale gelmektedir.

Anahtar Kelimeler: Güç elektroniği, güvenilirlik analizi, direnç toleransı, MIL-STD-217F, hata oranı tahmini, LED sürücü devresi.

INVESTIGATION OF THE EFFECT OF RESISTOR TOLERANCES ON SYSTEM RELIABILITY IN POWER ELECTRONICS CIRCUITS

Abstract

The present study employs a quantitative research methodology to investigate the effect of resistance tolerances on system reliability in power electronics circuits. Despite their frequent categorization as non-critical passive components, variations in manufacturing tolerances have the capacity to exert an indirect influence on circuit operating points, thereby inducing substantial alterations in the overall system failure rate. In this context, three different tolerance scenarios for resistor components were compared: minimum (±1%), nominal (tolerance neglected), and maximum (±10%). The comparison was made using a component stress model based on MIL-HDBK-217F standards.

The calculations yielded a system failure rate of 3.3685 FPMH and an estimated lifetime value of 296,868 hours for the minimum tolerance scenario. In the maximum tolerance scenario, the failure rate increased to 3.5618 FPMH, while the lifetime value decreased to 280,757 hours. In the nominal case, the failure rate was calculated as 3.4646 FPMH, and the estimated lifetime value was 288,634 hours. A 5.74% disparity in failure rate and a 16,111-hour discrepancy in lifetime were identified between the minimum and maximum tolerance scenarios.

The findings of this study demonstrate that even changes in resistance tolerance alone can have a measurable impact on the reliability indicators of the system. While resistance components do not constitute the primary source of failure in the system, in applications such as LED driver circuits characterized by high production volumes and extended operating times, these discrepancies assume economic and technical significance in terms of the overall reliability of the system.

Keywords: Power electronics, reliability analysis, resistor tolerance, MIL-STD-217F, failure rate prediction, LED driver circuits.

1. INTRODUCTION

The reliability of power electronics systems is determined by the interaction of component lifetime characteristics, manufacturing tolerances, duty profiles, and environmental stress factors (Wang & Blaabjerg, 2021; Bikash et al., 2022). This is particularly true in applications such as LED driver circuits, photovoltaic inverters, and electric vehicle power modules, where long-term and uninterrupted operation is paramount. Accurate estimation of failure rates is, therefore, critical for the development of effective design and maintenance strategies (Kalay et al., 2025; Zheng et al., 2025). Consequently, the modelling of parameters that affect system reliability, particularly the accurate calculation of the contribution of component tolerances to the system failure rate, has gained increasing importance in the power electronics literature in recent years (Okafor & Huitink, 2023; Navamani et al., 2024).

The extant literature has focused primarily on the failure mechanisms of critical components, such as semiconductors and capacitors. A plethora of exhaustive studies have been conducted on package failures, solder fatigue, and the hot spot behavior of semiconductors, including MOSFETs and IGBTs (Butnicu et al., 2025; Okafor & Huitink, 2023). In a similar vein, temperature- and voltage-sensitive lifetime models have been developed for aluminum electrolytic capacitors and MLCCs (Liu et al., 2023; Niu et al., 2018; Niu et al., 2020). Research conducted on capacitors indicates that this component can account for 60–80% of the total system failure rate (Liu et al., 2023; Niu et al., 2018).

Conversely, passive components such as resistors have frequently been regarded as "low risk" and have been disregarded in reliability analyses (DSIAC, 2023). However, variations in manufacturing tolerances have been shown to cause deviations in resistance values, thereby creating additional stress on other active components (Kuehl, 2009). This indirect effect has the potential to impact system lifetime. As stated by DSIAC, the failure modes of resistors can be categorized as follows: open circuit, parameter drift, moisture-induced degradation, and ESD/EOS-induced failures. The failure modes of resistors encompass open circuit, parameter drift, moisture-induced degradation, and ESD/EOS-induced failures (DSIAC, 2023).

Standards such as MIL-HDBK-217F, Telcordia SR-332, Siemens SN 29500, and FIDES have been extensively utilized in reliability modelling for a considerable duration (U.S. Department of Defense, 1995; Fermi National Accelerator Laboratory & INFN, 2021). Of these, MIL-HDBK-217F is frequently favoured during the design phase because it enables rapid failure rate estimation at the BOM level thanks to its part-stress multiplier model (π_T, π_P, π_Q, π_E) (Navamani et al., 2024). However, there is mounting criticism that these standards only partially reflect current component technologies and production tolerance effects (Butnicu et al., 2025).

Recent systematic reviews have clearly demonstrated a lacuna in the extant literature on the lifetime modelling of passive components (Okafor & Huitink, 2023; Liu et al., 2023). In particular, studies on the contribution of resistance tolerances to system failure rates are extremely limited in number. However, although this contribution is not as substantial as that of capacitors or semiconductors, it is quantifiable and significant for cost-effective reliability optimization (Wang & Blaabjerg, 2021; Zheng et al., 2025).

The present study aims to address this lacuna in the extant literature by means of a quantitative analysis of the effect of resistor tolerances on the total system failure rate, using an LED driver circuit as a case study. To this end, minimum, nominal, and maximum tolerance scenarios were evaluated using the MIL-HDBK-217F model, and the change in the system failure rate was examined using a Monte Carlo-based tolerance propagation method. This approach enables the quantitative separation of the effect of resistors, which are passive components, on reliability, and the clear demonstration of the reflection of tolerance narrowing/widening strategies on reliability performance.

2. MATERIAL AND METHOD

2.1. The present study investigates the system structure and operating environment

The present study was conducted on a grid-powered LED driver circuit, which is a common application in the field of power electronics. The objective of the present study is to employ quantitative methodologies to ascertain the impact of production tolerances on the total failure rate in the reliability analysis of the system. The circuit structure consists of an input rectifier stage, a passive filter stage, an active power factor correction (PFC) stage, a DC-DC converter stage, and an output filter. The system has been designed to operate at a nominal output power of 50 W under a 220 V AC, 50 Hz mains voltage. The circuit is mounted on a thermally balanced PCB, which is suitable for long-term (24/7) operating conditions. The system is an LED driver architecture consisting of rectifiers, input filter, PFC, and DC-DC stages. The general block diagram of this structure is shown in Figure 1 (Demir et al., 2018).

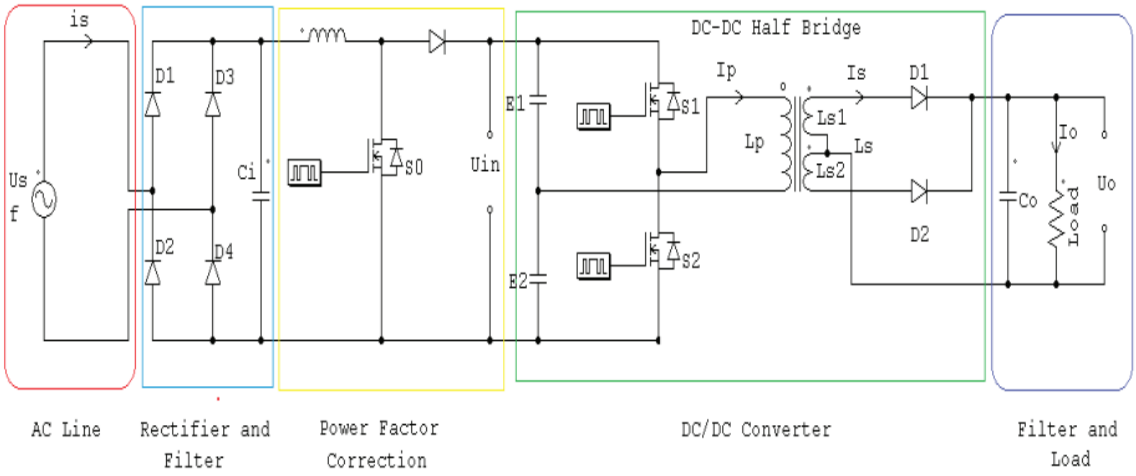


Figure 1: General diagram of LED driver circuit (Demir et al, 2018)

LED driver circuits are particularly sensitive systems in terms of reliability engineering due to their continuous operation and high energy efficiency requirements (Wang & Blaabjerg, 2021; Kalay et al., 2025). Although a significant proportion of such circuit failures are attributed to active semiconductors, various studies have reported that manufacturing tolerances in passive components can indirectly affect the system failure rate (Bikash et al., 2022; Okafor & Huitink, 2023). Even though resistors generally exhibit a low nominal failure rate, tolerance variations have the potential to affect current and voltage balance, thereby creating additional stress on other components (DSIAC, 2023; Kuehl, 2009).

2.2. The following section will address the components of resistors and the conditions under which they operate.

The study comprehensively analyzed all resistors, categorizing them as SMD thin-film type. A critical examination revealed their compliance with the IEC 60068 and JEDEC JESD22 standards. The maximum operating temperature recommended in the data sheets for these resistors is 155 °C. However, to more realistically reflect field conditions in the analyses, the maximum operating temperature was set to 50 °C. This choice is consistent with typical panel temperatures in LED driver circuits (Niu et al., 2018; Liu et al., 2023).

During the operation, the environmental conditions were accepted as GB (Ground Benign) class, as defined in the MIL-HDBK-217F standard. This is analogous to closed and temperature-controlled laboratory conditions.

2.3. Reliability Calculation Method

The MIL-HDBK-217F standard (U.S. Department of Defense, 1995) was used to calculate the failure rate (λ) of resistance components. This standard is based on the part-stress method, and the failure rate is defined as follows:

$$\lambda_{res} = \lambda_b * \Pi_T * \Pi_P * \Pi_S * \Pi_Q * \Pi_E \quad (1)$$

λ_b: Fundamental failure rate (FPMH),

Π_T: Temperature factor,

Π_P: Power stress factor,

Π_Q: Quality factor,

Π_E: Environmental factors.

In this study, the λ_b value was taken from the MIL-HDBK-217F table for thin film resistors (Navamani et al., 2024; Fermi National Accelerator Laboratory & INFN, 2021). The power stress ratio was assumed to be 50%, the quality factor was commercial grade, and the environmental factor was GB.

2.4. Tolerance Scenarios

Production tolerances in electronic systems cause deviations from the nominal values of circuit components, leading to changes in operating points and consequently in reliability indicators (Wang & Blaabjerg, 2021; Okafor & Huitink, 2023). This scenario can result in the gradual drift of system failure rates over time, particularly in continuous operational systems, such as LED driver circuits (Bikash et al., 2022). Consequently, a scenario-based approach was adopted to isolate the effect of resistance tolerances on system reliability.

The study evaluated three distinct tolerance scenarios:

- The minimum tolerance is indicated as ±1%. This configuration is indicative of a high-quality production line and is the scenario in which the lowest failure rate is expected.
- Nominal case (tolerance ignored): The reference scenario under consideration is one in which resistance values are assumed to be nominal and tolerance is not applied.
- The maximum tolerance, expressed as a ±10% margin, is indicated. This is indicative of the characteristics of low-cost components, and, notably, there is a wide range of production tolerances.

These scenarios enabled the isolation of the change in the system's total failure rate when the tolerance range was narrowed or widened. This method aligns with the voltage/temperature stress sensitivity-based approach that has been advocated in the extant literature for the reliability analysis of passive elements (DSIAC, 2023; Kuehl, 2009; Navamani et al., 2024).

The fundamental parameters associated with the tolerance scenarios are outlined in Table 1. The table presents the total failure rate, and life estimates for the system's three tolerance scenarios. The following conclusions can be drawn from the findings:

In the minimum tolerance scenario (±1%), the failure rate is 3.3685 FPMH, and the estimated life is 296,868 hours.

In the absence of any tolerance, the failure rate is 3.4646 FPMH, and the estimated lifetime is 288,634 hours.

In the maximum tolerance scenario (±10%), the failure rate increases to 3.5618 FPMH and the estimated lifetime decreases to 280,757 hours.

The findings of this study indicate a 5.74% discrepancy in failure rate and an approximate 16,111-hour disparity in lifetime between the minimum and maximum scenarios. As the tolerance range increases, a concomitant decrease in system reliability is observed. These disparities can become critical from economic and technical viewpoints, especially in systems that operate 24/7, such as LED driver circuits (Wang & Blaabjerg, 2021; Kuehl, 2009; DSIAC, 2023).

Tablo 1: Comparison of failure rate and system lifetime according to tolerance scenarios

Scenarios	Tolerance (%)	Total Failure Rate (FPMH)	Lifetime (hours)
Minimum Tolerance	±1	3.3685	296868
Nominal Tolerance	Tolerances-ignored	3.4646	288634
Maximum Tolerance	±10	3.5618	280757

2.5. Failure Rate Analysis and Data Processing

The failure rate evaluation was conducted using a transparent and reproducible approach based on MIL-HDBK-217F part stress methodology rather than relying on proprietary software tools. This methodology enables detailed and controllable analysis of how variations in resistor tolerances affect the overall reliability of the system and allows the results to be replicated in future studies without licensing constraints (Navamani et al., 2024; Butnicu et al., 2025; Okafor & Huitink, 2023).
The total system failure rate λ_{total} was calculated according to the classical series reliability model:

$$\lambda_{total} = \sum_{i=1}^{N} \lambda_i \quad (2)$$

where λi is the failure rate of each component. In this study, only resistor tolerance values were varied across scenarios, while all other component failure rates were fixed at their minimum tolerance values. This isolation ensured that the observed variations in λtotal could be attributed solely to resistor tolerances, thereby avoiding confounding effects from capacitors or other passive and active components (Wang & Blaabjerg, 2021; DSIAC, 2023).

The minimum, nominal (tolerance-ignored), and maximum tolerance scenarios were derived from pre-processed reliability data tables. Failure rates corresponding to resistor components were filtered and aggregated separately for each scenario. The percentage deviation from the nominal baseline was then calculated using:

$$\Delta\% = \frac{\lambda_{scenario} - \lambda_{nominal}}{\lambda_{nominal}} * 100 \quad (3)$$

The meantime to failure (MTTF) was estimated by converting the total system failure rate using the standard relationship:

$$MTTF(hours) = \frac{1000000}{\lambda_{total}} \quad (4)$$

Since failure rates were expressed in failures per million hours (FPMH), the results were processed and visualized using Python, with bar charts and pie charts used to highlight the magnitude of changes across tolerance scenarios.

Quantitatively, the minimum tolerance scenario (±1%) yielded a total failure rate of 3.3685 FPMH, corresponding to an MTTF of 296,868 h; the nominal (tolerance-ignored) scenario resulted in 3.4646 FPMH and 288,634 h; and the maximum tolerance scenario (±10%) gave 3.5618 FPMH and 280,757 h, respectively. This corresponds to a 5.74% difference in failure rate and a 16,111-h reduction in lifetime between the extreme scenarios.

These results clearly show that even minor changes in resistor tolerance bands can produce measurable shifts in overall system reliability. This finding emphasizes that tolerance selection should not be based solely on cost considerations but also integrated as a reliability-critical design parameter, particularly in

LED driver circuits that operate continuously (Wang & Blaabjerg, 2021; Okafor & Huitink, 2023; DSIAC, 2023; Navamani et al., 2024).

3. CONCLUSION

This study demonstrated that resistor tolerance variations, even in a narrow range between ±1% and ±10%, can cause measurable differences in the reliability performance of power electronic systems. The total system failure rate increased from 3.3685 FPMH to 3.5618 FPMH, and the predicted lifetime decreased from 296,868 h to 280,757 h across these tolerance extremes, indicating a 5.74% deviation in reliability solely attributable to resistor tolerance selection.

From an engineering design perspective, these results underline that tolerance selection should not be treated as a secondary decision. A tighter tolerance (e.g., ±1%) contributes to extending system lifetime by approximately 16,111 hours compared to a broad tolerance of ±10%. For LED driver circuits and other long-duty-cycle applications, this difference can translate to additional years of operational life without component replacement, improving both system uptime and end-user reliability.

From an economic standpoint, tighter tolerance resistors are typically more expensive on a per-unit basis. However, the extended lifetime and reduced failure rates can offset this cost through lower maintenance frequency, fewer warranty claims, and extended service intervals. In large production volumes, even modest improvements in reliability can yield significant total cost savings over the product life cycle.

In terms of maintenance and field performance, a broader tolerance band (e.g., ±10%) implies a higher probability of early-life deviations and accelerated wear-out behavior, potentially increasing the need for scheduled preventive maintenance or earlier component replacement. Conversely, tighter tolerance components enable longer maintenance intervals and more predictable failure behavior, which is particularly advantageous in critical infrastructure and continuous operation environments.

In conclusion, the findings highlight that resistor tolerance is a non-negligible design parameter that affects not only reliability metrics but also operational and economic outcomes. Incorporating tolerance selection into design-for-reliability strategies can enable more balanced trade-offs between initial component cost and lifecycle performance, particularly for high-volume and mission-critical power electronic systems.

REFERENCES

Bikash, S., Sprunck, S., & Jung, M. (2022). Reliability in power electronic systems: A hierarchical approach. IEEE Smart Grid Bulletin.

Butnicu, D., Grigore, M., & Oproescu, M. (2025). MTBF–PoL reliability evaluation and comparison using P/FMEA and reliability block diagrams. Electronics, 14(13), 2538. https://doi.org/10.3390/electronics14132538

Demir, M., Yildiz, A. B., & Ağir, T. (2018). Observation of the effects of electrostatic discharge and lightning surge on the reliability of a LED circuit driven by half-bridge converter. 2018 International Symposium on Power Electronics, Electrical Drives, Automation and Motion (SPEEDAM), 1073–1078. https://doi.org/10.1109/SPEEDAM.2018.8445297

DSIAC. (2023). Film resistor and capacitor failure modes and distributions (Technical brief). Defense Systems Information Analysis Center. https://dsiac.dtic.mil/technical-inquiries/notable/film-resistor-and-capacitor-failure-modes-and-distributions/

Fermi National Accelerator Laboratory & INFN. (2021). MIL-217, Bellcore/Telcordia and other reliability prediction models—Explained (Technical note). Fermilab. https://ad.fnal.gov/EPG/localincludes/Reliability_explained.pdf

Kalay, M. S., Erdemir, M., & Kaya, A. (2025). A systematic review on reliability and lifetime evaluation of power converters in power generation systems. IET Renewable Power Generation. https://doi.org/10.1049/rpg2.70111

Kuehl, R. W. (2009). Stability of thin-film resistors—Prediction and differences to experiences. Microelectronics Reliability, 49(9–11), 1234–1242. https://doi.org/10.1016/j.microrel.2008.12.006

Liu, H., Zhang, Q., & Sun, Y. (2023). Lifetime prediction and reliability analysis for aluminum electrolytic capacitors in EV charging modules based on mission profiles. Frontiers in Electronics, 4, 1226006. https://doi.org/10.3389/felec.2023.1226006

Navamani, D., Venkat, M., & Parthiban, P. (2024). Two decades of statistical approaches in reliability prediction. Microelectronics Reliability, 151, 115679. https://doi.org/10.1016/j.microrel.2024.115679

Niu, H., Wang, X., & Blaabjerg, F. (2018). Lifetime prediction of aluminum electrolytic capacitors in LED drivers. Microelectronics Reliability, 88–90, 1131–1135. https://doi.org/10.1016/j.microrel.2018.07.005

Niu, H., Wang, X., & Blaabjerg, F. (2020). Reliability-oriented optimization of aluminum electrolytic capacitors. Microelectronics Reliability, 109, 113669. https://doi.org/10.1016/j.microrel.2020.113669

Okafor, E. G., & Huitink, D. (2023). Failure mechanisms-driven reliability models for power electronics: A review. Journal of Electronic Packaging, 145(2), 020801. https://doi.org/10.1115/1.4055774

U.S. Department of Defense. (1995). MIL-HDBK-217F: Reliability prediction of electronic equipment (Notice 2). U.S. DoD. https://www.navsea.navy.mil/Portals/103/Documents/NSWC_Crane/SD-18/Test%20Methods/MILHDBK217.pdf

Wang, H., & Blaabjerg, F. (2021). Power electronics reliability: State of the art and outlook. Aalborg University. https://vbn.aau.dk/files/461497812/Power_Electronics_Reliability_State_of_the_Art_and_Outlook.pdf

Zheng, W., Li, X., & Zhao, Y. (2025). Reliability prediction of mixed-signal modules under complex conditions. Applied Sciences, 15(8), 4356. https://doi.org/10.3390/app15084356

KONDANSATÖR TOLERANSLARININ GÜÇ ELEKTRONİĞİ DEVRELERİNİN GÜVENİLİRLİĞİNE ETKİSİNİN İNCELENMESİ

MURAT DEMİR
İzmir Bakırçay University, Department of Electrical and Electronics Engineering,
murat.demir@bakircay.edu.tr, ORCID: 0000-0003-4407-9673

Özet

Güç elektroniği sistemlerinde, bileşen üretim toleransları nominal değerlerden sapmalara neden olabilir ve bu da zamanla devre çalışma noktalarında ve güvenilirlik ölçütlerinde değişikliklere yol açabilir. Bu etki, filtreleme ve enerji depolama işlevlerinin tolerans değişikliklerinden doğrudan etkilendiği LED sürücü devrelerinde kullanılan kondansatörler için özellikle önemlidir.

Bu çalışmada, MIL-HDBK-217F parça gerilme yöntemi kullanılarak kondansatör tolerans bantlarının sistem düzeyinde güvenilirlik üzerindeki etkisi değerlendirilmiştir. Üretici tolerans kodlarına göre üç tolerans senaryosu (minimum tolerans, nominal ve maksimum tolerans) tanımlanmıştır. Diğer bileşenler nominal değerlerde tutulurken, kondansatör tolerans etkilerini izole ederek arıza oranı hesaplamaları yapılmıştır.

Sonuçlar, toplam sistem arıza oranının 3,4393 FPMH (minimum tolerans) ile 3,4872 FPMH (maksimum tolerans) arasında değiştiğini ortaya koydu; bu, arıza oranında yaklaşık %1,38'lik bir artışa ve ömürde yaklaşık 4.000 saatlik bir azalmaya karşılık geliyor. Bu fark ılımlı görünse de, uzun ömürlü endüstriyel aydınlatma sistemlerinde önemli güvenilirlik ve maliyet etkileri yaratabilir.

Bu çalışma, kondansatör toleranslarının güvenilirlik açısından kritik bir tasarım parametresi olarak dikkate alınmasının önemini vurgulamaktadır. Daha sıkı toleranslı bileşenlerin seçilmesi, sistem ömrünü uzatabilir ve bakım sıklığını azaltabilir, böylece güvenilirlik odaklı LED sürücü tasarımı için pratik bir karar verme çerçevesi sağlayabilir..

Anahtar Kelimeler: Güç elektroniği, güvenilirlik analizi, kapasite toleransı, MIL-STD-217F, hata oranı tahmini, LED sürücü devresi.

IMPACT OF CAPACITOR TOLERANCES ON RELIABILITY OF POWER ELECTRONICS CIRCUITS

Abstract

In power electronic systems, component manufacturing tolerances can cause deviations from nominal values, leading to shifts in circuit operating points and reliability metrics over time. This effect is particularly critical for capacitors used in LED driver circuits, where filtering and energy storage functions are directly influenced by tolerance variations.

In this study, the impact of capacitor tolerance bands on system-level reliability was evaluated using the MIL-HDBK-217F part stress method. Three tolerance scenarios (minimum tolerance, nominal, and maximum tolerance) were defined based on manufacturer tolerance codes. Failure rate calculations were performed by isolating capacitor tolerance effects, while other components were kept at nominal values.

The results revealed that the total system failure rate varied from 3.4393 FPMH (minimum tolerance) to 3.4872 FPMH (maximum tolerance), corresponding to an approximately 1.38% increase in failure rate and nearly 4,000 hours reduction in lifetime. Although this difference appears moderate, it can result in significant reliability and cost impacts in long-lifetime industrial lighting systems.

This study highlights the importance of considering capacitor tolerances as a reliability-critical design parameter. Selecting tighter tolerance components can enhance system lifetime and reduce maintenance frequency, providing a practical decision-making framework for reliability-oriented LED driver design.

Keywords: Power electronics, reliability analysis, capacitor tolerance, MIL-STD-217F, failure rate prediction, LED driver circuits.

1. INTRODUCTION

Reliability in power electronics systems is directly related to the lifetime characteristics of the components utilised, the operating conditions, and the manufacturing tolerances. It is imperative to acknowledge the significance of capacitors within the context of system reliability, particularly in scenarios where circuits operate over extended periods and are subjected to elevated temperatures. The failure modes of different capacitor types, such as aluminium electrolytic, film, and MLCC, have been shown to have a significant effect on system failure rates through mechanisms such as ESR increase, capacitance loss, and dielectric breakdown (Niu et al., 2018; Okafor & Huitink, 2023).

A substantial body of research has been dedicated to the analysis of capacitor ageing processes and life estimation based on duty profiles (see Liu et al., 2023; Niu et al., 2020). The extant literature indicates that temperature, ripple current, and voltage stress are the primary factors that accelerate the degradation of capacitors. Nevertheless, the role of manufacturing tolerances in contributing to the system's overall error rate is frequently addressed in an indirect manner or overlooked. However, deviations from nominal capacitance values due to manufacturing tolerances have the potential to modify circuit characteristics, particularly in filtering and energy storage applications. This, in turn, can result in increased voltage fluctuations, stress profile shifts, and, consequently, an elevated error rate (Wang & Blaabjerg, 2021; DSIAC, 2023).

Although the tolerance effect is more pronounced in high-capacitance components, it can also contribute significantly to the system error rate in small capacitors, such as MLCCs, during long-term use. Consequently, the quantitative evaluation of the impact of capacitor tolerances in isolation addresses a significant gap in both reliability modelling and design decisions (Navamani et al., 2024; Butnicu et al., 2025).

2. MATERIAL AND METHOD

2.1. The present study investigates the system structure and operating environment

The present study investigates the effect of production tolerances of multiple capacitor components used in LED driver circuits on system reliability. LED drivers represent a significant test environment, wherein fluctuations in the failure rate attributable to passive elements can be distinctly discerned. This is attributable to the fact that these drivers are circuit structures subjected to uninterrupted operating profiles and elevated temperature conditions. The circuit's fundamental configuration comprises a rectifier stage, input filter capacitors, a switching stage, and an LED load group. The circuit diagram of the system is shown in Figure 1.

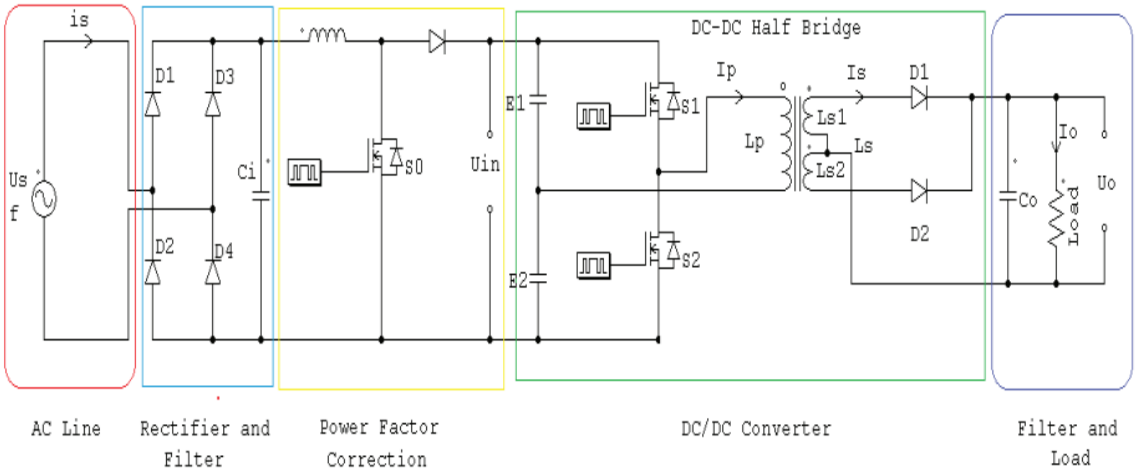


Figure 1: General diagram of LED driver circuit (Demir et al, 2017)

The circuit under consideration contains capacitors with differing capacitance values and dielectric types. These components can be categorised into three primary functional groups:

- Input filter capacitors: Low-capacitance surface-mount (SMD) capacitors (100 pF–470 nF) of the X7R or COG type are utilised for the suppression of electromagnetic interference (EMI) and the reduction of voltage ripple.
- DC-link capacitors: The utilisation of 820 µF electrolytic capacitors is imperative for the purpose of energy storage and stability.
- The following section will examine interlayer filter and bypass capacitors. The range of surface-mount device (SMD) capacitors comprises those with a value between 1 nF and 10 µF.

The production tolerance codes for these capacitors are defined by values such as K (±10%), M (±20%), J/F (±5%), and COG (±1%). Capacitance variations due to tolerance directly affect filtering efficiency and voltage stress, thereby altering the system's error rate. This phenomenon is particularly evident in X7R types, where tolerance-induced capacitance deviations become more pronounced at elevated temperatures, resulting in increased ripple voltage in DC-link capacitors (Liu et al., 2023; Wang & Blaabjerg, 2021; DSIAC, 2023).

The system is powered by a 220 V AC grid and modelled to operate at an ambient temperature of 60 °C. This temperature value has been demonstrated to cause an increase in the Pi_T temperature factor, thereby enabling more conservative results in error rate analyses. This approach is consistent with conditions corresponding to long-term industrial lighting applications. All analyses are based on the Ground Fixed (GF) environment class and apply the MIL-HDBK-217F standard.

2.2. The following section will address the components of resistors and the conditions under which they operate.

The capacitors utilised in the circuit have been evaluated within three primary categories: The following types of MLCC are available: X7R, COG and aluminium electrolytic. It is evident that MLCC capacitors are utilised in high-frequency filtering tasks, whereas electrolytic capacitors are employed for the purpose of energy storage and stability. Typical tolerance ranges according to capacitor types have been determined in accordance with the literature as COG: ±1%, J/F: ±5%, K: ±10%, and M: ±20% (Navamani et al., 2024; Okafor & Huitink, 2023).

Capacitance tolerances were incorporated into error rate calculations according to three scenarios:

The minimum tolerance is hereby stipulated as follows: The lower tolerance limit of the nominal value (for example, 90% for the K code) is defined as follows:

Nominal condition: The following scenario is presented herewith for consideration: in the event that tolerance is neglected, the maximum tolerance is as follows: The upper tolerance limit of the nominal value (e.g., 120% for the M code) is also indicated.

The minimum and maximum capacitance values were determined for each capacitor type based on the tolerance code. These values were reflected in the Pi_C factor used in the error rate formula. For instance, scenarios ranging from 656 µF to 984 µF were created under ±20% tolerance for 820 µF 63 V aluminium electrolytic capacitors. This situation exerts a substantial influence on the DC-link voltage stress factor (Pi_V) (Niu et al., 2018; Butnicu et al., 2025).

Given that the operating temperature is 60 °C, the temperature factor, designated Pi_T, was calculated for all capacitors based on this value. The voltage stress coefficient, denoted Pi_V, was determined based on the ratio of each capacitor's nominal voltage value (e.g., 25 V, 50 V, 63 V, 500 V) to the operating voltage. The estimation of error rate was contingent upon the ESR value and the dielectric type (X7R, X5R, COG, electrolytic).

The tolerance codes and types associated with the components were automatically extracted from the design list. Consequently, the error rate contribution of each capacitor was calculated individually, and the total system error rate was obtained as the sum of these values.

2.3. Reliability Calculation Method

The MIL-HDBK-217F standard (U.S. Department of Defense, 1995) was used to calculate the failure rate (λ) of resistance components. This standard is based on the part-stress method, and the failure rate is defined as follows:

$$\lambda_{cap} = \lambda_b * \Pi_T * \Pi_C * \Pi_V * \Pi_Q * \Pi_E \quad (1)$$

λ_b: Fundamental failure rate (FPMH),

Π_T: Temperature factor,

Π_C: Capacitance factor,

Π_V: Electrical stress factor for capacitor,

Π_Q: Quality factor,

Π_E: Environmental factors.

In this study, the λ_b value was taken from the MIL-HDBK-217F table for each capacitor. The quality factor was commercial grade, and the environmental factor was GB.

2.4. Tolerance Scenarios

Production tolerances have been shown to cause deviations from nominal values, particularly in passive components (e.g. resistors and capacitors) (Wang & Blaabjerg, 2021; Okafor & Huitink, 2023). These deviations have the potential to affect circuit operating points and system reliability. In the context of LED driver circuits, capacitors exhibit heightened sensitivity to tolerance deviations, a consequence of their critical functions in voltage ripple control, energy storage, and signal filtration. In order to evaluate the effect of capacitor tolerances on the system error rate, three basic scenarios were defined in this study.

- The minimum tolerance scenario is as follows: In circumstances where the nominal capacitance value is constrained to the lower tolerance limit (for example, 90% for K code, 80% for M code),
- Nominal scenario: The reference scenario under consideration is one in which tolerance is ignored, i.e. components operate at their nominal capacitance value.
- Maximum tolerance scenario: The nominal capacitance value is increased to the upper tolerance limit (e.g., 110% for K code, 120% for M code).

The scenarios under consideration were determined by taking into account the tolerance codes (K, M, J/F) associated with the various capacitor types (X7R, COG, electrolytic) utilised within the circuit. In each scenario, the relevant tolerance value was integrated into the failure rate calculation model (MIL-HDBK-217F), and both the capacitor group-specific and total system failure rates were calculated.

As illustrated in Table 1, the total failure rates and lifetime values of the capacitor group and the system are summarised according to the tolerance scenarios.

Tablo 1: Comparison of failure rate and system lifetime according to tolerance scenarios

Scenarios	Total Failure Rate (FPMH)	Lifetime (hours)
Minimum Tolerance	3.4393	290757
Tolerance-ignored	3.4646	288634
Maximum Tolerance	3.4872	286780

As illustrated in the table, the narrowing of the tolerance range (minimum scenario) has been shown to reduce the error rate while increasing system lifetime. Conversely, under maximum tolerance conditions, the error rate has been observed to increase, resulting in a reduction of approximately 3,977 hours in the system's operational lifespan. While this variation may appear negligible in absolute terms, it underscores the pivotal role that production tolerance can play in determining the reliability of industrial LED systems characterised by extended operational durations (Liu et al., 2023; DSIAC, 2023).

2.5. Failure Rate Analysis and Data Processing

The failure rate evaluation was conducted using a transparent and reproducible methodology based on the MIL-HDBK-217F part stress method, rather than relying on proprietary software tools. This approach facilitates a detailed and controlled evaluation of the impact of variations in capacitor tolerances on the overall reliability of the LED driver system. It also enables the analysis to be replicated without licensing constraints (Navamani et al., 2024; Butnicu et al., 2025; Okafor & Huitink, 2023).

The total system failure rate λ_{total} was calculated according to the classical series reliability model:

$$\lambda_{total} = \sum_{i=1}^{N} \lambda_i \quad (2)$$

where λi is the failure rate of each component.

In this study, only capacitor tolerance values were varied across scenarios, while all other component failure rates were fixed at their nominal values. This ensured that the observed variations in λ_{total}could be attributed solely to capacitor tolerances, thereby avoiding confounding effects from resistors or other passive and active components (Wang & Blaabjerg, 2021; DSIAC, 2023).

The minimum, nominal (tolerance-ignored), and maximum tolerance scenarios were derived from pre-processed reliability data tables corresponding to the entire capacitor population in the LED driver circuit. Capacitor failure rates were filtered and aggregated separately for each scenario. The percentage deviation from the nominal baseline was calculated as follows:

$$\Delta\% = \frac{\lambda_{scenario} - \lambda_{nominal}}{\lambda_{nominal}} * 100 \quad (3)$$

The meantime to failure (MTTF) was estimated by converting the total system failure rate using the standard relationship:

$$MTTF(hours) = \frac{1000000}{\lambda_{total}} \quad (4)$$

Since failure rates were expressed in failures per million hours (FPMH), the results were processed and visualized using MATLAB, with bar charts and pie charts used to highlight the magnitude of changes across tolerance scenarios.

For the minimum tolerance scenario, the total capacitor failure rate was 2.3795 FPMH, corresponding to a total system failure rate of 3.4393 FPMH and an MTTF of approximately 290,756.8 hours. For the nominal (tolerance-ignored) scenario, the total capacitor failure rate was 2.4048 FPMH, resulting in a total system failure rate of 3.4646 FPMH and an MTTF of 288,633.6 hours. For the maximum tolerance scenario, the capacitor failure rate increased to 2.4272 FPMH, with a total system failure rate of 3.4872 FPMH and an MTTF of 286,779.5 hours.

This corresponds to a 1.38 % relative variation in failure rate and a 3,977-hour difference in lifetime between the minimum and maximum tolerance scenarios. Although this shift may seem modest in absolute terms, in long-lifetime industrial lighting systems, such differences can translate into significant maintenance cost and reliability impacts over the operational lifetime of large deployments. These results clearly demonstrate that even moderate variations in capacitor tolerance bands can produce measurable shifts in overall system reliability. Therefore, tolerance selection should not be made solely based on cost, but also considered a reliability-critical design parameter, particularly in LED driver circuits that operate continuously (Wang & Blaabjerg, 2021; Okafor & Huitink, 2023; DSIAC, 2023; Navamani et al., 2024).

3. CONCLUSION

This study investigated the impact of capacitor tolerance variations on the reliability of an LED driver circuit under continuous operation. By isolating the tolerance parameter of capacitors and keeping other component failure rates fixed at their nominal values, the analysis clearly revealed how even moderate tolerance shifts can affect system-level failure behavior.

The results showed that the total system failure rate varied from 3.4393 FPMH in the minimum tolerance scenario to 3.4872 FPMH in the maximum tolerance scenario, with a nominal reference of 3.4646 FPMH. This difference corresponds to an approximate 1.38% change in failure rate and nearly 4,000 hours of lifetime reduction between the two extreme scenarios. Although this change appears moderate, its cumulative effect over long operational lifetimes—typical of industrial LED systems—can be significant in terms of maintenance cycles, service interruptions, and overall cost of ownership.

These findings emphasize that capacitor tolerance selection should not be based solely on cost or availability considerations. Instead, it must be integrated as a reliability-critical design parameter in power electronics applications. Selecting tighter tolerance capacitors can help increase system lifetime, reduce field failure rates, and lower total operational costs, particularly in LED driver circuits that operate 24/7 under thermal stress. Future studies may expand this approach by incorporating combined tolerance effects, thermal cycling, and mission-profile-based stress variations to further refine system-level reliability predictions.

REFERENCES

Butnicu, D., Grigore, M., & Oproescu, M. (2025). MTBF–PoL reliability evaluation and comparison using P/FMEA and reliability block diagrams. *Electronics, 14*(13), 2538. https://doi.org/10.3390/electronics14132538

Demir, M., İltir, M., & Yildiz, A. B. (2017). Determination of the effect of short-term interruptions in mains voltage on the reliability of consumer electronics products. 2017 IEEE International Conference on Environment and Electrical Engineering and 2017 IEEE Industrial and Commercial Power Systems Europe (EEEIC / I&CPS Europe), 1–5. https://doi.org/10.1109/EEEIC.2017.7977551

DSIAC. (2023). *Film resistor and capacitor failure modes and distributions* [Technical brief]. Defense Systems Information Analysis Center. https://dsiac.dtic.mil/technical-inquiries/notable/film-resistor-and-capacitor-failure-modes-and-distributions/

Kuehl, R. W. (2009). Stability of thin-film resistors—Prediction and differences to experiences. *Microelectronics Reliability, 49*(9–11), 1234–1242. https://doi.org/10.1016/j.microrel.2008.12.006

Liu, H., Zhang, Q., & Sun, Y. (2023). Lifetime prediction and reliability analysis for aluminum electrolytic capacitors in EV charging modules based on mission profiles. *Frontiers in Electronics, 4*, 1226006. https://doi.org/10.3389/felec.2023.1226006

Navamani, D., Venkat, M., & Parthiban, P. (2024). Two decades of statistical approaches in reliability prediction. *Microelectronics Reliability, 151*, 115679. https://doi.org/10.1016/j.microrel.2024.115679

Niu, H., Wang, X., & Blaabjerg, F. (2018). Lifetime prediction of aluminum electrolytic capacitors in LED drivers. *Microelectronics Reliability, 88–90*, 1131–1135. https://doi.org/10.1016/j.microrel.2018.07.005

Niu, H., Wang, X., & Blaabjerg, F. (2020). Reliability-oriented optimization of aluminum electrolytic capacitors. *Microelectronics Reliability, 109*, 113669. https://doi.org/10.1016/j.microrel.2020.113669

Okafor, E. G., & Huitink, D. (2023). Failure mechanisms-driven reliability models for power electronics: A review. *Journal of Electronic Packaging, 145*(2), 020801. https://doi.org/10.1115/1.4055774

U.S. Department of Defense. (1995). *MIL-HDBK-217F: Reliability prediction of electronic equipment* (Notice 2). U.S. DoD. https://www.navsea.navy.mil/Portals/103/Documents/NSWC_Crane/SD-18/Test%20Methods/MILHDBK217.pdf

Wang, H., & Blaabjerg, F. (2021). *Power electronics reliability: State of the art and outlook*. Aalborg University. https://vbn.aau.dk/files/461497812/Power_Electronics_Reliability_State_of_the_Art_and_Outlook.pdf

Zheng, W., Li, X., & Zhao, Y. (2025). Reliability prediction of mixed-signal modules under complex conditions. *Applied Sciences, 15*(8), 4356. https://doi.org/10.3390/app15084356

COMPARISON OF THE PERFORMANCE OF SWIN TRANSFORMER V2-B AND CNN MODELS IN DIABETIC RETINOPATHY CLASSIFICATION

Research Assistant KÜRŞAD KOCAİSPİR
Osmaniye Korkut Ata University, Electrical and Electronics Engineering Department, Osmaniye, Türkiye
kursadkocaispir@osmaniye.edu.tr, ORCID: 0009-0008-7640-3291

Prof. Dr. UFUK BAL
Osmaniye Korkut Ata University, Electrical and Electronics Engineering Department, Osmaniye, Türkiye
ufukbal@osmaniye.edu.tr, ORCID: 0000-0003-0345-6989

Lecturer EBUBEKİR AKKUŞ
Aydın Adnan Menderes University, Germencik Yamantürk Vocational School, Electronics and Automation Department, Aydın, Türkiye
ebubekir.akkus@adu.edu.tr, ORCID: 0000-0003-1232-948X

Abstract

Diabetic retinopathy (DR) is an eye disease that can cause vision loss if left untreated. However, with early detection and treatment, vision loss can be prevented. With the increase in artificial intelligence studies in recent years, research in medical image classification has also become widespread. Different deep learning methods are used to detect and classify DR. In this study, the DR classification performances of convolutional neural network (CNN)-based models and transformer-based models, which are widely used for DR classification, are investigated, and the obtained results are presented. For this purpose, five different pre-trained CNN models and a transformer model called Swin Transformer V2-B were trained and tested using the APTOS2019 dataset. According to the obtained results, the Swin Transformer V2-B model not only yielded higher accuracy with a test accuracy of 83.22% compared to the CNN models used in the study, but also provided significant improvements in precision, recall, and F1 score metrics.

Keywords: Swin Transformer V2-B, CNN, Diabetic Retinopathy, Image Classification

1. INTRODUCTION

Diabetic retinopathy (DR) is a serious complication associated with diabetes and can cause blindness if left untreated. This disease, caused by damage to the retinal vessels, often progresses asymptomatically in its early stages (Antonetti et al., 2012). Early diagnosis and regular eye examinations can prevent disease progression and significantly reduce the risk of vision loss (Aldebasi et al., 2015). As of 2010, more than 100 million people worldwide were affected by this complication, and this number is projected to exceed 190 million by 2030 (Zheng et al., 2012).

Deep learning (DL), a field of artificial intelligence, is used in a wide variety of tasks and has demonstrated significant success, particularly in image classification. CNNs, as a DL architecture, are particularly effective models for medical image classification thanks to their ability to learn hierarchical features. In the diagnosis of diabetic retinopathy (DR), they made significant contributions to early diagnosis and disease management by accurately classifying retinal images according to disease stages (Gulshan et al., 2016). Swin Transformer is a DL architecture that achieves high performance in visual recognition tasks at different levels of detail, such as image classification (image level), semantic segmentation (pixel level), and object detection (region level), by incorporating several visual priors into the vanilla transformer architecture to make it more suitable for various computer vision tasks (Liu et al., 2022).

A review of previous studies in the literature reveals that convolutional neural network (CNN)-based models are predominantly used for five-class DR classification, with some of these studies summarized below.

Gangwar and Ravi (2020) conducted a 5-class classification study of DR using the Inception-ResNet-v2 model on the Messidor-1 and APTOS2019 datasets. According to their results, they achieved 72.33% and 82.18% test accuracy on the Messidor-1 and APTOS2019 datasets, respectively, using the Inception-ResNet-v2 model. They emphasized that their study outperformed other published studies.

Achmad et al. (2021) conducted multi-class classification studies using a CNN model with the Messidor-1 and APTOS2019 datasets. CLAHE and Gaussian filtering methods were also used on the images in the dataset. According to the study results, they achieved 75% training accuracy, 73% validation accuracy, and 68% test accuracy.

Kumar et al. (2021) proposed DRISTI, a hybrid DL architecture incorporating VGG16 and a capsule network for multi-class DR classification. They achieved 75.50% validation accuracy with the model on an extended APTOS2019 dataset with five classes.

However, studies in the literature employ the ViT architecture for DR classification, and some of these studies is summarized below.

Dihin et al. (2023) conducted two- and five-class classification studies of DR using the APTOS2019 dataset and the Swin Transformer model. They applied a multiple wavelet transform to extract relevant features from images and introduced a different approach by incorporating the resulting images into the Swin Transformer model. According to the study results, their proposed method achieved 97.54% test accuracy for two-class classification and 82% for five-class classification.

Nazih et al. (2023) conducted five-class classification studies for DR using the fine-grained annotated diabetic retinopathy (FGADR) dataset and image transformers named ViT Base and ViT Large with 16 and 32 image patches, using different combinations of models. They achieved the highest classification accuracy of 82.50% with the method they proposed in their study.

Shoaib et al. (2025) conducted binary classification studies on DR using ViT with a dataset consisting of two classes: "Normal" and "Abnormal." According to the study results, their proposed method achieved 98.91% training accuracy, 98.79% validation accuracy, and 100% test accuracy for two-class classification.

In this study, to investigate the performance of the CNN and Swin Transformer models in DR classification and to compare the obtained results, five pre-trained CNN models (DenseNet101 ((Huang et al., 2017)), EfficientNetB0 (Tan and Le, 2019), MobileNetV3 (Howard et al., 2019), ResNet101 (He et al., 2016), and VGG16 (Simonyan and Zisserman, 2014)) and the Swin Transformer V2-B (Liu et al., 2022) model were trained separately on the APTOS2019 dataset. The trained models were then evaluated using classification metrics on a separate test dataset, and the performance impact of the Swin Transformer V2-B model on DR classification compared to the CNN models used in the study was analyzed.

The remainder of this article is organized as follows: Section 2 presents a detailed description of the materials and methods employed in this study, covering the dataset, the CNN architectures, and the Swin Transformer V2-B model. The hyperparameter values determined for the training of the trained DL models are presented, and the performance metrics used to evaluate their performance are explained. Section 3 describes the classification results obtained with the trained Swin Transformer V2-B and CNN models, and compares the performance of the Swin Transformer V2-B and CNN models based on these results. Section 4 summarizes the obtained results and discusses their implications.

2. MATERIALS AND METHODS

2.1. Dataset

This study used the APTOS2019 dataset (Kaggle, 2025), which consists of 3662 color fundus images and is publicly available on the Kaggle platform. The images in the APTOS2019 dataset are labeled for five different classes indicating DR severity: 0 (No DR), 1 (Mild), 2 (Moderate), 3 (Severe), and 4 (Proliferative DR). The distribution of images by class is shown in Table 1.

Table 1: The distribution of the number of images in the APTOS2019 dataset

Class Name	Number of Images
0 (No DR)	1805
1 (Mild)	370
2 (Moderate)	999
3 (Severe)	193
4 (Proliferative DR)	295

The dataset is divided into three different groups as 64% train, 16% validation and 20% test dataset.

2.2. CNN Models

CNN is a DL architecture that has achieved significant success, particularly in image classification (He et al., 2015). The LeNet-5 architecture revolutionized handwritten digit recognition, and AlexNet provided the early success of CNN-based methods (LeCun et al., 1998). The development of deeper architectures such as ResNet, GoogLeNet, and DenseNet has further enhanced the success of CNN architectures (Szegedy et al., 2015). Five different pre-trained CNN models were used in this study, and these models are briefly introduced below.

2.2.1. DenseNet121

DenseNet, a CNN model, was proposed by Huang et al. (2017). DenseNet121 has 121 layers and approximately 7 million parameters (Pillai et al., 2023).

2.2.2. EfficientNetB0

Developed in 2019 by Tan and Le, the model is the first and fundamental member of the EfficientNet family. It also has scaled variants of B0, B1, B2, and B7. It has approximately 5.3 million parameters (Tan and Le, 2019).

2.2.3. MobileNetV3

Introduced in 2019 by Howard and colleagues (Howard et al., 2019), MobileNetV3 is a CNN model optimized for portable devices. It has approximately 5.15 million parameters (Zhao and Wang, 2022).

2.2.4. ResNet101

ResNet101, introduced by He and colleagues in 2016, is a CNN architecture consisting of 101 layers with residual connections (He et al., 2016). The ResNet network uses residual connections through which gradients can pass directly; these connections prevent gradients from decaying to zero (Kalshetty and Parveen, 2023).

2.2.5. VGG16

VGG16 is introduced by Simonyan and Zisserman (2014), has 16 layers and approximately 138 million parameters in these layers (Simonyan and Zisserman, 2014). In all convolutional layers, the first step uses a 3x3 kernel filter, followed by a pooling layer (Albashish et al., 2021).

2.3. Swin Transformer V2-B

Swin Transformer V2 is a model introduced by Liu et al. (2022), using window-based self-attention to apply the Transformer architecture to visual data (Liu et al., 2022). Transformers use self-attention, which, unlike CNNs, do not have a strong inductive bias. Thanks to their self-attention mechanism,

transformers have advantages such as the competence to learn long-range dependencies and stronger modeling capacity (He et al., 2023).

The Swin Transformer V2-B model is a transformer model that was pre-trained using the ImageNet (ImageNet, 2025) dataset and has approximately 88 million parameters (Microsoft Research, 2025).

2.4. Hyperparameter values of CNN models and Swin Transformer V2-B

The hyperparameter values selected for training the DL models used in the study are shown in Table 2.

Table 2: The hyperparameter values selected for training the DL models used in the study

Deep Learning Model	*Epoch Number*	*Learning Rate*	*Batch Size*	*Optimizer*	*Loss Function*	*Seed Number*
DenseNet121	150	1e-06	16	Adam	CrossEntropy Loss	42
EfficientNetB0	150	1e-06	32	Adam	CrossEntropy Loss	42
MobileNetV3	150	1e-06	16	Adam	CrossEntropy Loss	42
ResNet101	150	1e-06	16	Adam	CrossEntropy Loss	42
VGG16	150	1e-06	8	Adam	CrossEntropy Loss	42
Swin Transformer V2-B	150	1e-06	32	Adam	CrossEntropy Loss	42

2.4. Performance Metrics

In this study, we used metrics accuracy, precision, recall, and F1 score, obtained from the test confusion matrix, to evaluate the performance of CNN models and the Swin Transformer V2 model. These metrics were calculated using the terms TP (True Positive), TN (True Negative), FP (False Positive), and FN (False Negative), which form the confusion matrices. The performance metrics used in the study can be calculated using equations (1), (2), (3), and (4) (Ayadi et al., 2021).

$$\text{Accuracy} = (TP + TN) / (TP+TN+FP+FN) \quad (1)$$

$$\text{Precision} = (TP) / (TP+FP) \quad (2)$$

$$\text{Recall} = (TP) / (TP+FN) \quad (3)$$

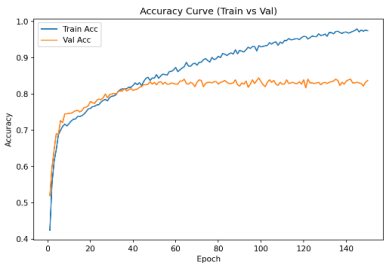
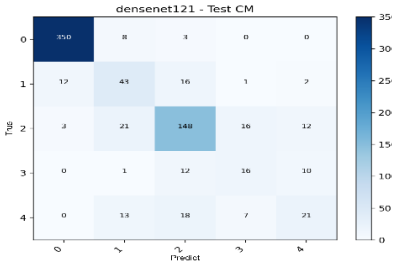
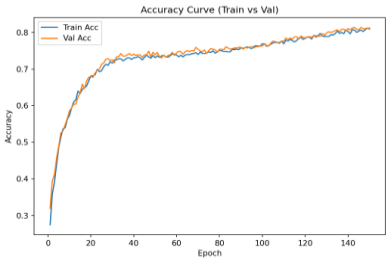
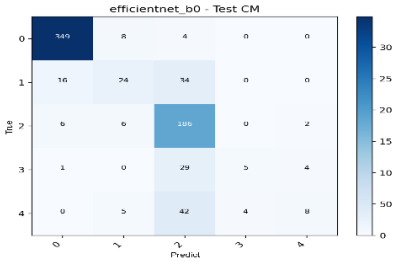
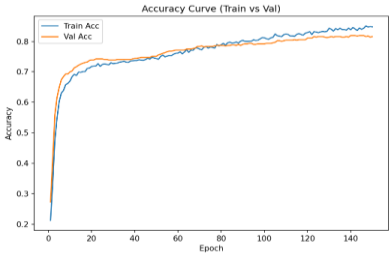
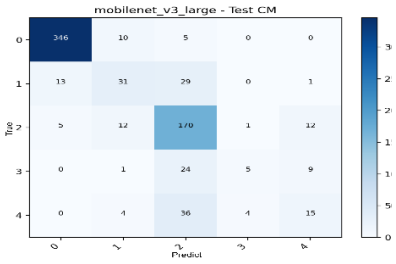
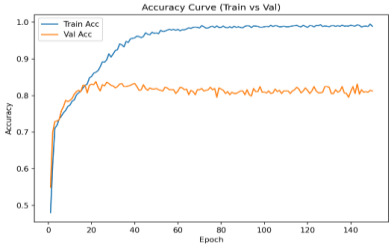
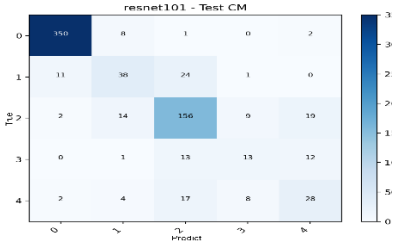
$$\text{F1-Score} = 2 \text{ x } (\text{Recall x Precision}) / (\text{Recall + Precision}) \quad (4)$$

3. EXPERIMENTAL RESULTS

In this study, a workstation equipped with 64 GB RAM, Intel i7-14700KF CPU, 1 TB NVMe SSD, and NVIDIA RTX A6000 GPU and Python 3.13 (Python, 2025) software were used.

3.1. Training CNN models

The accuracy curves of the trained CNN models are presented in Figure 1 along with the confusion matrices derived from the test dataset.

CNN Model	*Accuracy Curve*	*Confusion Matrix*
DenseNet121		
EfficientNetB0		
MobileNetV3		
ResNet101		

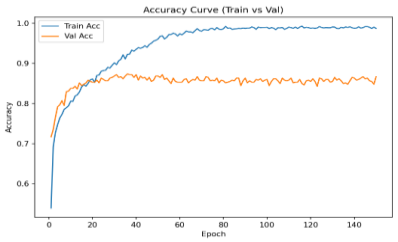
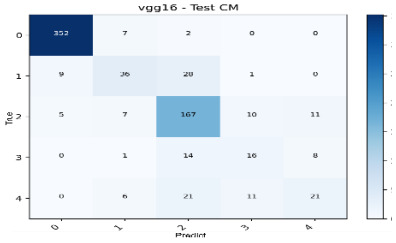
VGG16		

Figure 1: Accuracy curves of the trained CNN models and the confusion matrices obtained from the test dataset

The performance metric values of the trained CNN models, which were evaluated on the test dataset, were presented in Table 3.

Table 3: The performance metric values of CNN models

CNN Model	*Accuracy (%)*	*Precision (%)*	*Recall (%)*	*F1 Score (%)*
DenseNet121	78.85	61.54	61.14	61.12
EfficientNetB0	78.04	65.08	49.70	50.83
MobileNetV3	77.35	60.69	52.20	53.47
ResNet101	79.81	63.22	61.42	62.16
VGG16	80.76	65.18	61.25	62.62

3.2. Training Swin Transformer V2-B

Accuracy curves of the trained Swin Transformer V2-B and the confusion matrix obtained by testing them on the test dataset are shown in Figure 2.

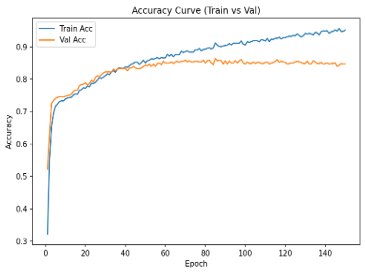
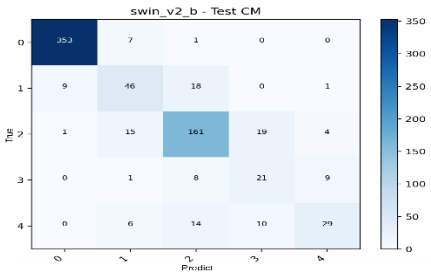
Transformer Model	*Accuracy Curve*	*Confusion Matrix*
Swin Transformer V2-B		

Figure 2: Accuracy curves of the trained Swin Transformer V2-B and the confusion matrices obtained by testing on the test dataset

The performance metric values of Swin Transformer V2-B trained on the test dataset are shown in Table 4.

Table 4: The performance metrics results of Swin Transformer V2-B

Transformer Model	*Accuracy (%)*	*Precision (%)*	*Recall (%)*	*F1 Score (%)*
Swin Transformer V2-B	83.22	69.54	68.69	68.68

3.3. Comparison of CNN models and Swin Transformer V2-B

Table 5 shows the performance metrics of CNN models and Swin Transformer V2-B models and the improvements achieved with the Swin Transformer V2-B model.

Table 5: The performance enhancement obtained with Swin Transformer V2-B

CNN Model	*Accuracy Increase (%)*	*Precision Increase (%)*	*Recall Increase (%)*	*F1 Score Increase (%)*
DenseNet121	4.37	8.00	7.55	7.56
EfficientNetB0	5.18	4.46	18.99	17.85
MobileNetV3	5.87	8.85	17.48	15.21
ResNet101	3.41	6.32	7.27	6.52
VGG16	2.46	4.36	7.44	6.06

As indicated by the values in Table 5, the Swin Transformer V2-B model achieved notable improvements in all performance metrics compared to the CNN models used in this study.

4. CONCLUSION

According to results in study, the Swin Transformer V2-B architecture demonstrates significant performance improvements across multiple evaluation metrics compared to traditional CNN models. Specifically, it achieves the high gains against MobileNetV3, with 5.87% improvement in accuracy, 8.85% in precision, 17.48% in recall, and 15.21% in F1 score. This demonstrates that Swin Transformer V2-B offers a superior balance of accurate predictions and minimized false negatives. Similarly, significant improvements are observed against EfficientNetB0, particularly in sensitivity 18.99% and F1-score 17.85%. According to the results, Swin Transformer V2-B not only achieved the highest test accuracy score of 83.22%, but also significantly improved other metrics. These findings demonstrate that Swin Transformer V2-B is a powerful alternative for image classification tasks requiring high performance.

Data Availability:

The APTOS2019 dataset used in this study is publicly available on the Internet at: https://www.kaggle.com/c/aptos2019-blindness-detection/.

Acknowledgment:

This work was supported by the Türkiye Sağlık Enstitüleri Başkanlığı [Health Institutes of Türkiye (TUSEB)] under Project No: 32082.

REFERENCES

Achmad, M. H., & RM, W. S. (2021, November). Diabetic Retinopathy Severity Level Classification Based on Fundus Image Using Convolutional Neural Network (CNN). In Seminar Nasional Informatika (SEMNASIF) (Vol. 1, No. 1, pp. 173-185).

Albashish, D., Al-Sayyed, R., Abdullah, A., Ryalat, M. H., & Almansour, N. A. (2021, July). Deep CNN model based on VGG16 for breast cancer classification. In *2021 International conference on information technology (ICIT)* (pp. 805-810). IEEE.

Aldebasi, Y. H., Reddy, P. R., Nair, V. G., & Ahmed, M. I. (2015). Screening for diabetic retinopathy: the optometrist's perspective. Clinical Optometry, 1-14.

Antonetti, D. A., Klein, R., & Gardner, T. W. (2012). Diabetic retinopathy. New England Journal of Medicine, 366(13), 1227-1239.

Ayadi, W., Elhamzi, W., Charfi, I., & Atri, M. (2021). Deep CNN for brain tumor classification. Neural processing letters, 53(1), 671-700.

Dihin, R. A., AlShemmary, E., & Al-Jawher, W. (2023). Diabetic retinopathy classification using swin transformer with multi wavelet. Journal of Kufa for Mathematics and Computer, 10(2), 167-172.

Gangwar, A. K., & Ravi, V. (2020). Diabetic retinopathy detection using transfer learning and deep learning. In Evolution in Computational Intelligence: Frontiers in Intelligent Computing: Theory and Applications (FICTA 2020), Volume 1 (pp. 679-689). Singapore: Springer Singapore.

Gulshan, V., Peng, L., Coram, M., Stumpe, M. C., Wu, D., Narayanaswamy, A., ... & Webster, D. R. (2016). Development and validation of a deep learning algorithm for detection of diabetic retinopathy in retinal fundus photographs. jama, 316(22), 2402-2410.

He, Y., Nath, V., Yang, D., Tang, Y., Myronenko, A., & Xu, D. (2023, October). Swinunetr-v2: Stronger swin transformers with stagewise convolutions for 3d medical image segmentation. In International Conference on Medical Image Computing and Computer-Assisted Intervention (pp. 416-426). Cham: Springer Nature Switzerland.

He, K., Zhang, X., & Sun, J. (2015). Delving deep into rectifiers: Surpassing human-level performance on ImageNet classification. Proceedings of the IEEE International Conference on Computer Vision (ICCV), 1026–1034.

He, K., Zhang, X., Ren, S., & Sun, J. (2016). Deep residual learning for image recognition. In Proceedings of the IEEE conference on computer vision and pattern recognition (pp. 770-778).

Howard, A., Sandler, M., Chu, G., Chen, L. C., Chen, B., Tan, M., ... & Adam, H. (2019). Searching for mobilenetv3. In Proceedings of the IEEE/CVF international conference on computer vision (pp. 1314-1324).

Huang, G., Liu, Z., Van Der Maaten, L., & Weinberger, K. Q. (2017). Densely connected convolutional networks. In Proceedings of the IEEE conference on computer vision and pattern recognition (pp. 4700-4708).

ImageNet. (2025, September 05). ImageNet. https://www.image-net.org/

Kaggle (2025, September 15). APTOS 2019 Blindness Detection. https://www.kaggle.com/competitions/ aptos2019-blindness-detection/data

Kalshetty, R., & Parveen, A. (2023). Abnormal event detection model using an improved ResNet101 in context aware surveillance system. Cognitive Computation and Systems, 5(2), 153-167.

Kumar, G., Chatterjee, S., & Chattopadhyay, C. (2021). DRISTI: a hybrid deep neural network for diabetic retinopathy diagnosis. Signal, Image and Video Processing, 15(8), 1679-1686.

LeCun, Y., Bottou, L., Bengio, Y., & Haffner, P. (1998). Gradient-based learning applied to document recognition. Proceedings of the IEEE, 86(11), 2278-2324.

Liu, Z., Hu, H., Lin, Y., Yao, Z., Xie, Z., Wei, Y., ... & Guo, B. (2022). Swin transformer v2: Scaling up capacity and resolution. In Proceedings of the IEEE/CVF conference on computer vision and pattern recognition (pp. 12009-12019).

Microsoft Research. (2025, September 05). Swin Transformer. https://github.com/microsoft/Swin-Transformer

Nazih, W., Aseeri, A. O., Atallah, O. Y., & El-Sappagh, S. (2023). Vision transformer model for predicting the severity of diabetic retinopathy in fundus photography-based retina images. IEEE Access, 11, 117546-117561.

Pillai, R., Sharma, N., Gupta, R., & Sharma, A. (2023, May). Classification of plant diseases using DenseNet 121 transfer learning model. In 2023 International Conference on Advances in Computing, Communication and Applied Informatics (ACCAI) (pp. 1-6). IEEE.

Python (2025, September 20). Python 3.13.0. https://www.python.org/downloads/release/python-3130/

Shoaib, M. R., Esmaiel, H., Al Ayidh, A., Hussein, H. S., & Abd El-Samie, F. E. (2025). Automated diabetic retinopathy classification using vision transformers on optical confocal microscopy images. Applied Optics, 64(28), 8151-8160.

Simonyan, K., & Zisserman, A. (2014). Very deep convolutional networks for large-scale image recognition. arXiv preprint arXiv:1409.1556.

Szegedy, C., Liu, W., Jia, Y., Sermanet, P., Reed, S., Anguelov, D., ... & Rabinovich, A. (2015). Goingdeeper with convolutions. In Proceedings of the IEEE conference on computer vision and pattern recognition (pp. 1-9).

Tan, M., & Le, Q. (2019, May). Efficientnet: Rethinking model scaling for convolutional neural networks. In International conference on machine learning (pp. 6105-6114). PMLR.

Zhao, L., & Wang, L. (2022). A new lightweight network based on MobileNetV3. KSII Transactions on Internet & Information Systems, 16(1).

Zheng, Y., He, M., & Congdon, N. (2012). The worldwide epidemic of diabetic retinopathy. *Indian journal of ophthalmology*, *60*(5), 428-431.

NANO HYDROXYAPATITE-REINFORCED COLLAGEN HYDROLYSATE FILMS FROM LEATHER WASTE WITH IMPROVED WATER BARRIER PERFORMANCE

Assist. Prof. Dr. LEVENT INANC
Denizli Vocational School of Technical Sciences, Pamukkale University, Denizli, Turkiye
E-Mail: leventinanc@gmail.com, ORCID: 0000-0002-4564-7671

Prof Dr. BUGRA OCAK
Faculty of Engineering, Department of Leather Engineering, Ege University 35100, Bornova, Izmir, Turkiye
E-Mail: bugra.ocak@ege.edu.tr, ORCID: 0000-0002-8082-4290

Abstract

The tannery industry faces a significant challenge in sustainably managing solid waste, as the large amounts of hazardous materials it generates—particularly collagen-rich leather fiber residues such as trimming waste—can be valorized by incorporation into film production, thereby mitigating environmental pollution. At the same time, increasing awareness of the environmental impact of petroleum-based plastics has led to heightened research interest in bioactive and biodegradable packaging system. Collagen hydrolysate (CH) was obtained from leather industry trimming waste through enzymatic hydrolysis, whereas SDS-PAGE analysis verified that the resulting hydrolysate possessed a type I structure. Hydroxyapatite, a major mineral component of bone tissue, exhibits high biocompatibility and bioactivity. With the aim of enhancing water barrier properties, CH-based films were evaluated for thickness, moisture content (MC, %), water solubility (WS, %), and water vapor permeability (WVP) following the incorporation of hydroxyapatite nanoparticles. The addition of 4% hydroxyapatite nanoparticles increased film thickness from 0.131 mm to 0.159 mm, while reducing MC and WS from 19.302% to 12.556% and from 37.016% to 21.232%, respectively, indicating improved water resistance. WVP similarly decreased from 1.649 to 1.073 × 10^{-11} g/Pa·h·m. These findings indicate that CH-based films containing hydroxyapatite nanoparticles can serve as environmentally friendly functional packaging materials.

Keywords: leather, waste, collagen, hydroxyapatite, film.

1. INTRODUCTION

Over the last few decades, the combined effects of rapid industrialization and intensified economic growth have contributed to a pronounced escalation in the amount of tannery solid waste generated (Sharma and Vuppu, 2024; Muralidharan et al., 2024). The leather industry, a sector of global economic importance, has a considerable environmental impact owing to its resource-intensive and chemically intensive production processes, wherein every 1000 kg of raw hide produces roughly 800 kg of solid waste, with only 200 kg ultimately yielding finished leather (Khan et al., 2025; Sharma and Vuppu, 2024). During the pre-tanning phase, the leather manufacturing process generates a considerable amount of trimming residues from the contouring and classification of hides, which, in the absence of an efficient solid waste management system, are often indiscriminately discarded despite being rich in proteins, primarily type I collagen (Maliha et al., 2024; Muralidharan et al., 2024).

Synthetic polymeric waste, predominantly produced from plastic-based packaging materials, has emerged as a critical environmental issue, substantially contributing to global plastic waste leakage. The magnitude of this issue is underscored by the 400.3 million metric tons of plastic waste produced worldwide in 2022, approximately 150 million metric tons of which originated from the packaging industry (Latorre et al., 2025; Sierra et al., 2025). Recognized for their advantageous functional and structural characteristics, protein-based biopolymers derived from biological sources have emerged as principal raw materials in the fabrication of biodegradable packaging materials, thereby driving the development of environmentally sustainable alternatives to conventional petroleum-based plastics

owing to their outstanding biocompatibility, degradability, and renewability (Latorre et al., 2025; Bagri et al., 2025).

Among biopolymers, natural materials such as collagen and synthetic polymers like polyvinyl alcohol have garnered attention as viable alternatives due to their biodegradability (Bagri et al., 2025). Collagen, an animal-derived fibrous protein characterized by its unique triple-helical structure, is the most abundant protein in vertebrates and is extensively distributed across various biological tissues—including skin, tendons, bones, cartilage, ligaments, and blood vessels—exhibiting remarkable film-forming capacity and inherent biodegradability that together impart superior mechanical strength to collagen-based packaging materials (Ran et al., 2025; Andonegi et al., 2025). Nevertheless, the practical application of pristine collagen-based packaging films is hindered by their relatively open polymeric network, resulting in suboptimal mechanical stability and poor water barrier performance, particularly due to their high degree of WS (Shi et al., 2025; Maliha et al., 2024; Muralidharan et al., 2024).

The integration of nanomaterials into polymeric film matrices has been demonstrated to significantly improve water barrier properties by facilitating robust interfacial interactions with the biopolymer network. Owing to their remarkable surface reactivity and large specific surface area, the incorporation of nanoparticles represents an effective approach for enhancing the functional performance of films (Cai et al., 2025; Salimiraad et al., 2022). Hydroxyapatite (HA), a stoichiometric calcium phosphate compound with the formula $Ca_{10}(PO_4)_6(OH)_2$, serves as the predominant inorganic phase in vertebrate bones and teeth and, owing to its exceptional biocompatibility, bioactivity, and structural similarity to natural bone, has been extensively investigated for diverse biomedical and composite material applications (Okuno et al., 2025; Ghegoiu et al., 2025).

The primary objective of this study is to develop a sustainable packaging material that mitigates the escalating use of plastic products by valorizing trimming waste generated from the leather industry. This study focused on investigating the effect of CH based films obtained from leather industry trimming wastes on water barrier properties using HA.

2. MATERIAL AND METHOD

2.1. Material

All reagents, including sodium hydroxide (NaOH, ≥ 97.0%), acetic acid (≥ 99.7%), pepsin (lyophilized powder, ≥ 3,200 units/mg protein), petroleum ether, β-mercaptoethanol (≥ 99.0%), Coomassie Brilliant Blue R-250, methanol (≥ 99.8%), calcium chloride ($CaCl_2$, ≥ 93%), and nano-hydroxyapatite (< 200 nm particle size, ≥ 97%), were obtained from Sigma-Aldrich.

2.2. Methos

2.3. Preparation of collagen hydrolysate from leather trimming waste

To preserve the integrity of the samples during transportation to the laboratory, trimming waste specimens were sealed in polyethylene bags and placed within a polystyrene container at a sample-to-ice ratio of 1:3 (w/w), after which the samples were washed, drained, and weighed upon arrival before being re-sealed in polyethylene bags and stored at −18 °C until further analyses. Thawed in a refrigerator at 4–5 °C overnight prior to analysis, the frozen trimming waste samples were prepared for subsequent procedures, and after the removal of visible fat and hair, they were carefully washed with cold water to eliminate residual impurities. Following fat extraction with petroleum ether for 3 h using a Soxhlet apparatus in accordance with AOAC Method 945.16, the trimming waste was weighed and stored in a refrigerator until further use.

2.4. Obtainment of collagen hydrolysate from leather trimming waste

CH was extracted from 20 g of defatted, dried trimming waste by the addition of 100 mL of 0.1 M NaOH, followed by continuous stirring of the mixture at 25 °C for 40 min. The alkali-treated pellets were thoroughly washed with distilled water for 10 min to eliminate residual salts and guarantee the complete removal of alkaline residues. After adjusting the pH of the pretreated trimming waste to 2.0 with 0.2 M acetic acid and subjecting it to enzymatic treatment with pepsin (0.125%, 3200 units/mg), the mixture was hydrolyzed at 37 °C under continuous agitation at 120 rpm, and the CH was subsequently extracted in a temperature-controlled water bath for 6 h with sustained stirring at the same

rate. After enzyme inactivation by heating at 90 °C for 10 min and centrifugation of the crude CH solution at 11,000 × g for 15 min, the supernatant was preserved at −18 °C overnight, subsequently freeze-dried for 48 h, and the obtained powder was weighed and stored at 4 °C until further utilization.

2.5. Electrophoresis analysis of collagen hydrolysate from leather trimming waste

Each proteolyzed hide sample (10 µL) was combined with 5× loading buffer containing β-mercaptoethanol at a 1:2 (v/v) ratio—prepared by mixing 50 µL of β-mercaptoethanol with 950 µL of sample buffer—and subsequently incubated in a water bath at 95 °C for 5 minutes prior to electrophoretic separation on 12% resolving and 4% stacking gels. Protein electrophoresis was conducted using the Mini-PROTEAN Tetra System (Bio-Rad Laboratories, USA), initially operated at a constant current of 15 mA per gel for 15 min and subsequently increased to 25 mA per gel until the dye front reached the lower edge of the resolving gel. The gel was then stained with 0.1% (w/v) Coomassie Brilliant Blue R-250 in a solution containing 15% (v/v) methanol and 5% (v/v) acetic acid for 2 hours, followed by destaining in 30% (v/v) methanol and 10% (v/v) acetic acid. Pre-stained protein molecular weight standards were utilized to determine the molecular weight profile of the CH obtained from the enzymatically hydrolyzed trimming waste.

2.6. Fabrication of collagen hydrolysate based films containing different ratios of hydroxyapatite

To ensure complete dissolution, a 6% (w/v) CH solution was prepared by dissolving 6 g of CH in 100 mL of distilled water under continuous stirring at 40 °C for 1 h. Glycerol (30% of the dry polymer weight) was then added to the film-forming solution. Gradually added at different ratios of 1%, 2%, 3%, and 4% to CH-based films and ultrasonically mixed for 20 min to ensure uniform distribution, the resulting mixture was then magnetically stirred at 40 °C for 5 min, followed by degassing to remove entrapped air bubbles. After careful casting into a circular mold (12 cm in diameter), 25 mL of the CH film-forming solution was dried at 40 °C under controlled conditions for 18 h to yield the fully formed film.

2.7. Characterization of collagen hydrolysate-based/polyvinyl alcohol films incorporating varying ratios of hydroxyapatite

2.7.1. Film thickness

The average thickness of each CH-based film was calculated after measuring film thickness with a vernier caliper at five randomly selected points, with measurements performed in quintuplicate.

2.7.2. Moisture content

The CH films were oven-dried at 37 °C for 48 hours until a constant weight was achieved, and for each film, the initial (mi) and final (mf) weights were measured and documented. MC (%) analyses were performed in triplicate to ensure experimental reliability, and the MC (%) was calculated using the following equation.

$$Moisture\ content\ (\%) = \frac{m_i - m_f}{m_i} \times 100$$

2.7.3. Water solubility

Following determination of its initial dry weight (m_i) by oven-drying at 105 °C for 12 h, the 2 cm × 2 cm CH-based film sample was immersed in 100 mL of deionized water for 24 h, after which it was removed and oven-dried at 105 °C until a constant weight (mf) was attained for WS (%) analysis. To ensure reproducibility, all WS (%) measurements of the CH-based films were performed in triplicate and determined using the following equation.

$$Water\ solubility\ (\%) = \frac{m_i - m_f}{m_i} \times 100$$

2.7.4. Water vapor permeability

Assessed in accordance with the ASTM E96–95 standard method with minor modifications, the WVP of the CH-based films was determined by mounting 3.5 cm-diameter film disks onto 50 mL vials containing 2 g of silica gel to maintain a relative humidity of 0 % within the vials. Following incubation at 25 °C for 24 h under controlled conditions with relative humidity maintained at 75 % using a saturated NaCl solution, vial weights were recorded, and WVP (g / Pa h m) was calculated as the average of three replicates.

$$Water\ vapor\ permeability = \frac{\text{mass of water permeated (g)} \times \text{thickness (m)}}{\text{permeation area } (m^2) \times \text{time (h)} \times \text{vapor pressure difference (Pa)}}$$

3. Results and Discussion

3.1. Electrophoresis analysis of CH obtained from leather TW

The results of SDS-PAGE analysis are presented in Fig. 1. Employing a polyacrylamide gel as the supporting matrix, SDS-PAGE facilitates the separation of denatured, linearized protein molecules according to their molecular weight, governed by charge-dependent migration differences (Yu et al., 2025). As illustrated in Fig. 1, the molecular weight distribution of CH was determined to range between 106 and 175 kDa, and the protein pattern of CH/in demonstrated three well-defined and intense bands at approximately 175, 117, and 106 kDa, corresponding to the β, α1, and α2 chains of type I collagen, respectively.

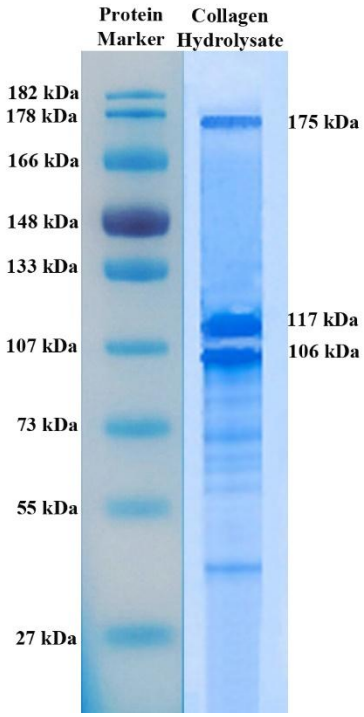


Figure 1: SDS-PAGE characterization of the CH profile.

The protein profile of type I collagen comprises a β band, indicative of a dimer formed either through the association of α1 and α2 chains or by the linkage of two α chains, and additionally exhibits the characteristic α1 and α2 bands arising from its triple-helical configuration, which consists of two α1 chains and one α2 chain (Filipe et al., 2024).

3.2. Thickness

Film thickness constitutes a critical parameter for evaluating the structural and functional attributes of the samples, and it markedly affects the mechanical properties, barrier performance, and overall efficacy of biopolymer films in packaging applications (Priyadharshee and Preetha, 2023). The results of the film thickness evaluation for CH-based biodegradable films prepared with varying HA concentrations are presented in Table 1. The incorporation of HA was observed to induce significant alterations in film thickness, which ranged from 0.136 mm to 0.159 mm, relative to the control sample.

Table 1: Thickness values of control and CH-based film samples containing different ratios of HA.*

Film samples	Thickness (mm)
CH	0.131 ± 0.003^{f}
CH/HA$^{\%1}$	0.136 ± 0.002^{e}
CH/HA$^{\%2}$	0.141 ± 0.003^{d}
CH/HA$^{\%3}$	0.151 ± 0.005^{c}
CH/HA$^{\%4}$	0.159 ± 0.004^{b}

*Distinct letters within the same column indicate statistically significant differences among sample groups, as determined by the Duncan test at $p < 0.05$.

Thool et al. (2025) ascribed the observed variations in film thickness to the interfacial interactions among the polymeric constituents within the film matrix, which consequently influence the structural integrity and overall morphology of the films.

3.3. Moisture content

The functional performance of packaging films and the quality of the packaged products are both critically influenced by their MC (%) (Zhang et al., 2025). Under conditions of elevated humidity, CH-based films can absorb water and swell, leading to reduced mechanical integrity and impaired protective performance. Table 2 summarizes the MC (%) of CH-based films containing hydroxyapatite nanoparticles at different concentrations (1%, 2%, 3%, and 4% v/v).

Table 2: Moisture content (%) values of control and CH-based film samples containing different ratios of HA.

Film samples	MC (%)
CH	19.302 ± 0.564^{a}
CH/HA$^{\%1}$	17.853 ± 0.681^{b}
CH/HA$^{\%2}$	16.314 ± 0.196^{c}
CH/HA$^{\%3}$	14.757 ± 0.622^{d}
CH/HA$^{\%4}$	12.556 ± 0.198^{e}

*Distinct letters within the same column indicate statistically significant differences among sample groups, as determined by the Duncan test at $p < 0.05$.

The incorporation of hydroxyapatite nanoparticles, which fill the voids in the film matrix and consequently reduce the capacity for water retention, resulted in significant differences ($p < 0.05$) in the MC (%) of the films across formulations, with CH recording the highest value (19.302%) and CH/HA4% the lowest (12.556%).

3.4. Water solubility

Reducing solubility is essential for preserving performance stability under humid conditions, as WS (%) of packaging films serves as a key indicator of their ability to maintain structural integrity in aqueous environments. CH-based films displayed a high WS of 37.016% (Table 3); however, the addition of hydroxyapatite nanoparticles significantly decreased solubility ($p < 0.05$). This decrease is mainly ascribed to enhanced intermolecular interactions, such as hydrogen bonding and electrostatic forces, between the nanoparticles and the CH matrix, which promote the formation of a denser and more water-resistant film structure.

Table 3: Water solubility (%) values of control and CH-based film samples containing different ratios of HA.

Film samples	**WS (%)**
CH	37.016 ± 0.861^{a}
CH/HA$^{\%1}$	33.088 ± 0.905^{b}
CH/HA$^{\%2}$	28.072 ± 0.648^{c}
CH/HA$^{\%3}$	24.292 ± 0.588^{d}
CH/HA$^{\%4}$	21.232 ± 0.868^{e}

*Distinct letters within the same column indicate statistically significant differences among sample groups, as determined by the Duncan test at $p < 0.05$.

3.5. Water vapor permeability

The efficiency of films in protecting packaged products from moisture-induced deterioration is reflected by WVP, which serves as a critical parameter in packaging applications. Table 4 presents the WVP results of CH-based films, whereas the control CH film exhibited a high value of $1.649 \pm 0.081 \times 10^{-11}$ g/Pa·h·m. The incorporation of hydroxyapatite nanoparticles significantly decreased the WVP of CH-based films ($p < 0.05$).

Table 4: Water vapor permeability values of control and CH-based film samples containing different ratios of HA.

Film samples	**WVP ($\times 10^{-11}$ g / Pa h m)**
CH	1.649 ± 0.081^{a}
CH/HA$^{\%1}$	1.544 ± 0.052^{b}
CH/HA$^{\%2}$	1.451 ± 0.043^{c}
CH/HA$^{\%3}$	1.370 ± 0.049^{d}
CH/HA$^{\%4}$	1.073 ± 0.092^{e}

*Distinct letters within the same column indicate statistically significant differences among sample groups, as determined by the Duncan test at $p < 0.05$.

CH-based films exhibited enhanced hydrophobicity, as hydroxyapatite nanoparticles reinforced the matrix and promoted the formation of a denser network that inhibits moisture diffusion.

3. CONCLUSION

CH-based films derived from leather industry trimming waste were successfully fabricated with varying ratios of hydroxyapatite nanoparticles, resulting in improved water barrier properties and highlighting their potential as sustainable biodegradable packaging alternatives. Revealed by the results, the incorporation of hydroxyapatite nanoparticles significantly enhanced the water barrier properties of the CH-based films. As the hydroxyapatite nanoparticle content increased, reductions in MC (%), WS (%), and WVP were observed in CH-based films, resulting in a denser and more hydrophobic film structure.

REFERENCES

Andonegi, M., Diez, A.G., Costa, C.M., Romanyuk, K.N., Kholkin, A.L., de la Caba, K., Guerrero, P., Lanceros-Mendez, S., (2025). Piezoelectric properties of collagen films: Insights into their potential for electroactive biomedical applications, International Journal of Biological Macromolecules, 309(1), 142799.

Bagri, F., Pircheraghi, G., Riahi, Z., Imani, M., Rhim, J.W. (2025). Multifunctional gelatin/polyvinyl alcohol composite films integrated with sulfur quantum dots and silica nanohybrid for active packaging of fruits, Journal of Environmental Chemical Engineering, 13(5), 118289.

Cai, X., Chen, L.Q., Yang, X., Wang, Y.L., Xu, J.X., Zhang, R.F., Ling, S.L., Liu, Y.Y. (2025). Active curcumin-loaded γ-cyclodextrin-metal organic frameworks as nano respiratory channels for reinforcing chitosan/gelatin films in strawberry preservation, Food Hydrocolloids, 159, 110656.

Filipe, M.S., André, R., Ferreira, M., Diaz-Lanza, A.M., André, V., Alves, M.M., Pacheco, R., Rijo, P. (2024). Valorizing sardine scales: a circular approach to sustainable collagen for cosmetics and nutrition applications, Frontiers in Pharmacology, 15, 1443358.

Ghegoiu, L., Predoi, D., Iconaru, S.L., Ciobanu, C.S., Rokosz, K., Raaen, S., Badea, M.L., Predoi, M.V. (2025). Physicochemical and preliminary biological properties of thin films based on fluoride-doped hydroxyapatite in a dextran matrix for biomedical applications, Coatings, 15(5), 565.

Khan, S., Hossain, M.S., Khan, M.A., Akhi, A.R., Ali, M.F. (2025). Preparation and Characterization of Eco-friendly Polymer Composites from Leather Wastes, South African Journal of Chemical Engineering, 54, 461-469.

Latorre, M.E., Ravazzoli, P.D., Velazquez, D.E. (2025). Mechanical, surface, and thermal properties of gelatin-collagen blend films with potential application to biodegradable packaging, International Journal of Food Properties, 28(1), 2540851.

Liang, X., Feng, S.Y., Ahmed, S., Qin, W., Liu, Y.W. (2019). Effect of potassium sorbate and ultrasonic treatment on the properties of fish scale collagen/polyvinyl alcohol composite film, Molecules, 24(13), 2363.

Maliha, M., Rashid, T.U., Rahman, M.M. (2024). Fabrication of collagen-sodium alginate based antibacterial and edible packaging material: Performance evaluation using Entropy-Combined Compromise Solution (CoCoSo), Carbohydrate Polymer Technologies and Applications, 8, 100582.

Muralidharan, V., Jebathomas, C.R.T., Sundaramoorthy, S., Madhan, B., Palanivel, S. (2024). Preparation and evaluation of novel biodegradable Kombucha cellulose-based multi-layered composite tableware, Industrial Crops and Products, 215, 118629.

Okuno, Y., Terakawa, S., Ujitsugu, A., Ikeda, M., Hayashi, K., Tanaka, T., Sawa, G., Kohama, T., Kusunoki, M. (2025). Selective growth of c- and a-axis-oriented hydroxyapatite thin films by sputtering, Vacuum, 239, 114409.

Priyadharshee, M., Preetha, R. (2023). Fabrication and characterization of gelatin-based nanocomposite edible film prepared from eggshell with anthocyanin as pH indicator to assure quality of food, Journal of Food Science and Technology-Mysore, 60(4), 1389-1401.

Ran, R.M., Luo, X.Y., Zhai, D.M., He, Y.Q., Guo, X., He, L.J., Li, G.Y. (2025). Development of a dual-layer collagen film with insulating, antioxidant, antimicrobial, and pH-sensitive

properties for the maintenance and visual monitoring of shrimp freshness, Food Hydrocolloids, 169, 111603.

Salimiraad, S., Safaeian, S., Basti, A.A., Khanjari, A., Nadoushan, R.M. (2022). Characterization of novel probiotic nanocomposite films based on nano chitosan/nano cellulose/gelatin for the preservation of fresh chicken fillets, LWT-Food Science and Technology, 162, 113429.

Sharma, N., Vuppu, S. (2024). A sustainable approach for conversion of leather trimming wastes into non-edible gelatine and its physicochemical analysis, optimization, FTIR, XRD characterization, and statistical study, Biomass Conversion and Biorefinery, https://doi.org/10.1007/s13399-024-05940-4

Shi, X., Ju, F.X., Wang, R.X., Xu, J., Li, T.D., Wei, T., Lv, A., Yang, H. (2025). Brilliant fabrication of multifunctional collagen-based packaging films with rigid-flexible coupling structure bio-inspired by pangolins, Food Chemistry, 479, 143814

Sierra, K., Siddique, A., Dudley, A., Garner, L.J., Kassama, L.S., Cho, S.E., Peng, Y.C., Morey, A. (2025). Engineering a sustainable packaging film using poultry collagen for the food industry, Applied Food Research, 5(2), 101314.

Thool, O.K., Sasidharan, A., Krishna, B.M., Sabu, S., Navaf, M., Sunooj, K.V. (2025). Nano-hydroxyapatite (n-HAP) from Pangasius bone side streams and its application as a reinforcing agent in biodegradable food packaging films, Sustainable Food Technology, 3(1), 227-238.

Wang, K.H., Yang, X.J., Liang, J.J., Rong, Y., Zhao, W.J., Ding, J.H., Liu, Y.M., Liu, Q. (2024). Preparation, characterization, antimicrobial evaluation, and grape preservation applications of polyvinyl alcohol/gelatin composite films containing zinc oxide@quaternized chitosan nanoparticles, International Journal of Biological Macromolecules, 277(4), 134527.

Yontar, A.K., Çevik, S., Yontar, O. (2023). Green production of plant/collagen-based antibacterial polyvinyl alcohol (PVA) nanocomposite films, Sustainable Chemistry and Pharmacy, 33, 101119.

Yu, S.W., Kim, H.J., Jang, J.H., Kim, K.T., Ahn, D.U., Paik, H.D. (2025). Ovomucoid hydrolysates produced by pepsin stimulate immune activity of RAW 264.7 macrophages via the MAPK/NF-κB pathway, Enzyme and Microbial Technology, 190, 110710.

Zhang, C., Jiang, K., Lin, Y.L., Cui, R., Wu, H. (2025). Preparation and characterization of d-carvone-doped chitosan-gelatin bifunctional (antioxidant and antibacterial properties) film and its application in xinjiang ramen, Foods, 14(15), 2645